



---

Chair of Structural Mechanics  
Technische Universität München

Master's Thesis Nr.: 225

Investigation of Periodic Structures for the Design of Acoustic  
Metamaterials Using Unit-Cell Modeling

Jose Daniel Perez Ramirez

Master's Thesis  
for the Master of Science program Computational Mechanics

Matriculation number : 03669007  
Referent : Univ.-Prof. Dr.-Ing. Gerhard Müller  
Supervisors : M.Sc. Matthias Miksch  
M.Sc. Quirin Aumann  
Date of issue : June 15, 2017  
Date of submission : November 20, 2017



# Abstract

Acoustic metamaterials are artificial structures that have emerged due to the increased manipulation of their mechanical properties. This allows for a wide range of applications, such as in vibration abatement or in the manipulation of acoustic waves. Typically, they consist of periodic substructures called unit-cells. As a whole, they behave like a continuous material, which enables the material to develop tailored properties that can differ significantly from properties generally observed in nature. To achieve such materials, proper mathematical modeling has to be performed. The most common approach is based on the use of structures whose interaction with mechanical waves is dominated by the internal behavior of a single unit-cell.

In order to investigate the design characteristics of acoustic metamaterials, this master's thesis examines the methods used to study the low-to-mid frequency dynamics of one-, two- and three-dimensional periodic structures. For that reason, a computational tool that provides the dispersion relation based on the these methods is developed. Furthermore, numerous numerical experiments are performed to validate the tool and to gain insight into new designs of acoustic metamaterials.

Keywords:

- Acoustic metamaterials
- Band gaps
- Band structure
- Dispersion curves
- Periodic structures
- Unit-cell modeling
- Vibro-acoustic insulation
- Wave finite element method

# Declarations

## Acknowledgements

I would like to express my deepest thanks to my parents, brothers and girlfriend. Without their support, wisdom, encouragement and understanding during my studies, it would have been impossible for me to finish this work. My special gratitude is to my supervisor Matthias Miksch, for his guidance at all stages of my work. His knowledge and hints were essential to me for completing this thesis.

## Declaration

With this statement I declare, that I have independently completed this Master's thesis. The thoughts taken directly or indirectly from external sources are properly marked as such. This thesis was not previously submitted to another academic institution and has also not yet been published.

München, November 20, 2017

Jose Daniel Perez Ramirez

# Contents

<b>Abstract</b>	<b>III</b>
<b>Declarations</b>	<b>IV</b>
<b>List of Figures</b>	<b>VII</b>
<b>List of Symbols</b>	<b>X</b>
<b>1 Introduction</b>	<b>1</b>
1.1 Motivation . . . . .	1
1.2 Goals . . . . .	2
1.3 Outline of the thesis . . . . .	2
<b>2 Fundamentals</b>	<b>3</b>
2.1 Fundamentals of vibration theory . . . . .	3
2.1.1 Free vibration of undamped systems . . . . .	3
2.1.2 Description of damping in discrete systems . . . . .	5
2.1.3 Tuned mass dampers . . . . .	6
2.1.4 Basic concepts of structural waves . . . . .	7
2.2 Periodic structures . . . . .	9
2.2.1 Potential of periodic structures in engineering . . . . .	9
2.2.2 Methods of analysis for periodic structures . . . . .	10
2.3 One-dimensional wave finite element method . . . . .	11
2.3.1 Floquet's theorem . . . . .	12
2.3.2 Unit-cell dynamics . . . . .	13
2.3.3 Direct approach . . . . .	13
2.3.4 LR method . . . . .	18
2.3.5 Zhong's method . . . . .	18
2.3.6 Condensed wave finite element method . . . . .	19
2.3.7 Dispersion curves . . . . .	21
2.3.8 Inverse approach . . . . .	22
2.4 Two-dimensional wave finite element method . . . . .	23
2.4.1 Bloch's theorem and wave propagation . . . . .	24
2.4.2 Boundary conditions for two-dimensional unit-cell . . . . .	26
2.4.3 Irreducible Brillouin contour and band structure . . . . .	27
2.4.4 Inverse approach . . . . .	28
2.5 Three-dimensional wave finite element method . . . . .	29
2.5.1 Inverse approach . . . . .	31

<b>3 Implementation and validation</b>	<b>33</b>
3.1 Implementation . . . . .	33
3.2 Benchmark problem for one-dimensional unit-cell . . . . .	36
3.2.1 Infinite Euler-Bernoulli beam . . . . .	36
3.2.2 Infinite Euler-Bernoulli beam with a punctual mass . . . . .	40
3.2.3 Infinite Euler-Bernoulli beam with a spring-mass system . . . . .	41
3.2.4 Infinite Euler-Bernoulli beam with a TMD . . . . .	42
3.2.5 Comparison of methods . . . . .	43
3.3 Benchmark problem for two-dimensional unit-cell . . . . .	44
3.3.1 Plate . . . . .	44
3.4 Benchmark problem for three-dimensional unit-cell . . . . .	46
3.5 Numerical errors . . . . .	47
<b>4 Numerical experiments</b>	<b>50</b>
4.1 Analysis of an acoustic black hole in one dimension . . . . .	50
<b>5 Summary and conclusions</b>	<b>57</b>
<b>A Appendix</b>	<b>59</b>
A.1 Graphical User Interface . . . . .	59
A.2 MATLAB® code . . . . .	60
A.3 Python code . . . . .	64
A.4 ANSYS® code . . . . .	64
A.5 Compact disk . . . . .	65
<b>Bibliography</b>	<b>66</b>

# List of Figures

2.1	Periodic structure as an assembly of identical unit-cells of length $L_x$ . . . . .	9
2.2	Floquet's boundary definition in a unit-cell . . . . .	12
2.3	One-, two- and three-dimensional unit-cell models with their respective left and right boundary under one-dimensional wave propagation. . . . .	14
2.4	Interaction between two unit-cells . . . . .	16
2.5	Type of waves in positive direction . . . . .	17
2.6	Two-dimensional unit-cell with its respective degrees of freedom . . . . .	24
2.7	Schematic representation of a unit-cell in an arbitrary position within an infinite two-dimensional periodic structure . . . . .	25
2.8	Irreducible Brillouin zone in a two-dimensional unit-cell . . . . .	27
2.9	Three-dimensional unit-cell with its respective degrees of freedom at the corners	30
2.10	Three-dimensional unit-cell with its respective degrees of freedom at the edges	30
2.11	Three-dimensional unit-cell with its respective degrees of freedom at the faces	31
3.1	Coupling of nodes between two unit-cells . . . . .	33
3.2	Flowchart of the code implementation for the extraction of $\mathbf{M}$ , $\mathbf{C}$ and $\mathbf{K}$ from ANSYS® . . . . .	34
3.3	Flowchart of the code implementation for the tool METAMAT . . . . .	35
3.4	Dispersion curves of the freely propagating waves in positive direction from 0 to 100 Hz of an infinite Euler-Bernoulli beam modeled with different type of elements . . . . .	36
3.5	Band structure of the first two bands of an infinite Euler-Bernoulli beam . .	37
3.6	Dispersion curves of the freely propagating waves in positive direction from 0 Hz to 100 Hz of a one-dimensional model using different solvers . . . . .	38
3.7	Dispersion curves of the freely propagating waves in positive direction from 0 Hz to 100 Hz of a two-dimensional model using different solvers . . . . .	38
3.8	Dispersion curves of the freely propagating waves in positive direction from 0 Hz to 100 Hz of a three-dimensional model using different solvers . . . . .	38
3.9	Dispersion curves of the freely propagating waves in positive direction from 0 to 5000 Hz of a one-dimensional model using different solvers . . . . .	39
3.10	Dispersion curves of the freely propagating waves in positive direction from 0 to 5000 Hz of a two-dimensional model using different solvers . . . . .	39
3.11	Dispersion curves of the freely propagating waves in positive direction from 0 to 5000 Hz of a three-dimensional model using different solvers . . . . .	39
3.12	Dispersion curves of the freely propagating waves in positive direction from 0 to 50 Hz of a one-dimensional model with an added mass of 0.156 kg using different solvers . . . . .	40

3.13	Dispersion curves of the freely propagating waves in positive direction from 0 to 50 Hz of a one-dimensional model with a punctual mass. The mass has different values to see the effect of increasing mass . . . . .	40
3.14	Dispersion curves of the freely propagating waves in positive direction from 0 to 50 Hz of a one-dimensional model with an spring-mass system using different solvers. The spring-mass system consists of a mass of 0.156 kg and a spring of 1000 N/m . . . . .	41
3.15	Dispersion curves from 0 to 50 Hz of one-dimensional model with a spring-mass system. The curves show that the resonance frequency of the resonator appears before the stop band and the increasing of the bandwidth for vibration reduction as the stiffness raises . . . . .	41
3.16	Dispersion curves from 0 to 100 Hz of one-dimensional model with a TMD .	42
3.17	Dispersion curves from 0 to 100 Hz of one-dimensional model with a TMD. The plots show the influence of three different values of damping ratios for the attached TMD . . . . .	42
3.18	Computational time of the analysis of a one-dimensional model with 300 degrees of freedom using different solvers vs the number of steps . . . . .	43
3.19	Computation time of the analysis of a one-dimensional model with different solvers vs the number of degrees of freedom . . . . .	43
3.20	Band structure of a plate. The two first bands are shown along the irreducible Brillouini contour. . . . .	44
3.21	Band structure of a plate with different configurations . . . . .	45
3.22	Band structure of a plate with a punctual mass in the center. The value of the mass is variable . . . . .	45
3.23	Band structure of a plate with a spring-mass system. The value of the spring stiffness is variable . . . . .	46
3.24	Band structure of a three-dimensional unit-cell. The first band is shown along the irreducible Brillouini contour . . . . .	47
3.25	Dispersion curves from 0 to 100 Hz of the one-dimensional model of an infinite Euler-Bernoulli beam with numerical errors due to the size of the element . .	48
3.26	Dispersion curves from 0 to 5000 Hz of the one-dimensional model of an infinite Euler-Bernoulli beam with discretization errors . . . . .	48
3.27	Dispersion curves from 20 to 30 Hz of the three-dimensional model of an infinite Euler-Bernoulli beam with errors due to the element selection . . . . .	49
4.1	Main design parameters of an acoustic black hole . . . . .	50
4.2	Acoustic black hole with different values of exponential taper coefficient $exp$ .	51
4.3	Acoustic black hole with an additional thin layer . . . . .	51
4.4	Dispersion curves from 0 to 1000 Hz of one-dimensional undamped unit-cells with different exponential taper coefficient . . . . .	52
4.5	Dispersion curves from 0 to 2000 Hz of a one-dimensional undamped black hole with and without additional layer of material . . . . .	53
4.6	Dispersion curves from 0 to 2000 Hz of a one-dimensional undamped black hole with exponential taper coefficient equals to 2.2. The figure shows the dispersion curves of unit-cells with different layer properties . . . . .	54

4.7	Dispersion curves from 0 to 500 Hz of a one-dimensional undamped black hole with different materials and exponential taper coefficient equals to 2.2 . . . . .	55
4.8	Dispersion curves from 0 to 500 Hz of a one-dimensional titan black hole with different values of damping ratio and exponential taper coefficient . . . . .	56
A.1	Layout of METAMAT . . . . .	60
A.2	Simplified UML diagram of the implementation of analyzed model . . . . .	60
A.3	Simplified UML diagram of the implementation of approaches used by the WFEM . . . . .	61
A.4	Simplified UML diagram of the implementation of the visualization . . . . .	61

# List of Symbols

## Superscripts

$T$	Vector/matrix transpose
$red$	Reduced vector or matrix
$*T$	Complex conjugate transpose of a matrix
*	Reduced matrix by model order reduction

## Subscripts

$B$	Subscript related to all nodes at the boundary
$f$	Index related to forces/momenta
$H$	Subscript related to hybrid coordinates
$I$	Subscript related to all internal nodes
$k$	Index related to the wave modes
$max$	Maximum
$L$	Subscript related to all nodes at the left boundary
$N$	Position of unit-cell index
$q$	Index related to displacements/rotations
$R$	Subscript related to all nodes at the right boundary
$r$	Mode index
$s$	Mode index
$x$	Propagation direction
$y$	Propagation direction
$z$	Propagation direction

## Matrix and vectors

<b>C</b>	Damping matrix
<b>D</b>	Dynamic stiffness matrix
<b>F</b>	Vector of external loads (forces/moments)
<b>I</b>	Identity matrix
<b>K</b>	Stiffness matrix
<b>k</b>	Propagation vector
<b>L</b>	Matrix used for the formulation of the eigenvalue problem
<b>M</b>	Mass matrix
<b>N</b>	Matrix used for the formulation of the eigenvalue problem
<b>q</b>	Vector of displacements/rotations
<b>R</b>	Reduction matrix
<b>r</b>	Vector of displacements/rotations in reduced basis
<b>S</b>	Symplectic matrix
<b>T</b>	Transfer matrix
<b>Z</b>	Zero matrix
<b><math>\kappa</math></b>	Wave vector
<b><math>\Phi</math></b>	Eigenvector
<b><math>\phi</math></b>	Eigenvector partition
<b><math>\Psi_I</math></b>	Fixed interface modes
<b><math>\Theta</math></b>	Craig-Bampton matrix
<b>0</b>	Zero vector

## Greek letters

$\alpha$	$1/s$	Alpha damping constant
$\beta$	$s$	Beta damping constant
$\lambda$	$m$	Wavelength
$\delta_{rs}$		Kronecker delta
$\Delta$	$m$	Length of unit-cell
$\kappa$	$rad/m$	Wave number
$\mu$		Eigenvalues which represent the wave types
$\nu$		Poisson's ratio
$\omega$	$rad/s$	Angular frequency
$\omega_E$	$rad/s$	Eigenfrequencies

---

$\rho$	$kg/m^3$	Density
$\zeta_r$		Modal damping ratio

## Latin letters

$A$	$m^2$	Cross-sectional area
$A_r$	$kg$	Generalized mass of mode $r$
$D$	$Pa \cdot m^3$	Flexural rigidity
$E$	$N/m^2$	Young's modulus
$e$		Euler's number
$f$	Hz	Frequency
$G$	$N/m^2$	Shear modulus
$I$	$m^4$	Second moment of inertia
$i$		Imaginary unit
$k$		Propagation constant
$m_H$		Index related to the number of rows
$N_R$		Number of retained basis functions
$n$		Number of degrees of freedom in the cross section
$n_H$		Index related to the number of columns
$p$		Total number of degrees of freedom
$t$	$s$	Time
$v$	$m/s$	Speed
$v_l$	$m/s$	Wave speed of longitudinal waves
$v_s$	$m/s$	Wave speed of shear waves
$v_b$	$m/s$	Wave speed of bending waves in thin beams
$v_p$	$m/s$	Wave speed of bending waves in plates

## Other notations

Bold fond-weight	Vector and matrices
Normal font-weight	Scalars
$\sim$	Dynamic condensation
$\hat{\cdot}$	Denotes reduction of the matrix
$\cdot$	Denotes first derivative with respect to time
$\cdot\cdot$	Denotes second derivative with respect to time

# 1 Introduction

## 1.1 Motivation

Today, periodic structures are observed on many engineering systems. One example is the so-called acoustic metamaterial, which has tailored dynamic properties that can differ significantly from properties observed in nature. Acoustic metamaterials have many engineering applications, such as in the attenuation of noise caused by vibrating structural components or the improvement of acoustic performance. Therefore, the prediction of their dynamic performance plays an important role in the design of many products.

Methods based on the so-called wave finite element method have to be investigated, since they lead to the decomposition of the propagating waves into a wave basis. This wave basis is associated to the propagation constants, which provide useful information about how the waves propagate through a structure and also give a straightforward way to identify the frequency ranges where no free wave propagation takes place. The most important milestones are presented in the following table:

Year	Author	Contribution
1887	Rayleigh	First study of continuous periodic structures
1929	Bloch	Bloch wave theory
1960	Mead	Pioneering works in dynamic of periodic structures
1969	McDaniel	Proposal of the transfer matrix method
1974	Orris and Petyt	Proposal of the wave finite element method
1992	Langley	Force boundary conditions for two-dimensional periodic structures
1994	Zhong	Symplectic eigenproblem
2005	Mace	Finite element prediction of wave motion in structural waveguides
2005	Phani	Works in wave propagation in two-dimensional periodic lattices
2008	Manconi	Wave propagation modeling in two-dimensional structures
2013	Claeys	Analysis of tuned resonators to obtain low-frequency stop bands
2014	Zhou	Condensed wave finite element method

**Table 1.1:** Time-line of the most important studies in engineering periodic structures

Based on the above-mentioned developments, it is possible then to develop computational tools to design acoustic metamaterials. These tools have to be capable of accurately dealing with the low-to-mid frequency dynamics of complex models, and with a computational time that allows the evaluation of performance of different designs of acoustic metamaterials. Therefore, this thesis integrates the available methods in order to model periodic structures so that their dynamic properties can be manipulated.

## 1.2 Goals

The goal of this thesis is to develop a finite element tool to analyze the dispersion relation of general periodic structures to evaluate different designs of acoustic metamaterials. The tool will then be used to gain insights in the design of metamaterials, such that they satisfy specific requirements on their frequency dependent performance.

Besides providing a literature overview of the available methods to model periodic structures, the work involves the following steps:

- Creation of a computational tool with ANSYS® and MATLAB® to compute the dispersion diagrams of one-dimensional infinite structures.
- Extension of the tool for two- and three-dimensional periodic structures.
- Evaluation of different designs of acoustic metamaterials to validate the tool.
- Investigation of an acoustic black hole as acoustic metamaterial in one dimension.

## 1.3 Outline of the thesis

Chapter 2 presents the necessary theory of mechanical vibrations, wave propagation, and periodic structures. There is also a literature review of the available formulations to model the dynamic behavior of damped or undamped periodic structures in one, two, and three dimensions. Chapter 3 discusses the algorithmic approach, implementation aspects, and validation of the computational tool. Numeric experiments are then performed in Chapter 4, to gain insight in the design of acoustic black holes. The discussion is closed by some concluding remarks in Chapter 5. The MATLAB® code and ANSYS® models used can be found in the CD attached.

## 2 Fundamentals

This chapter provides an overview of the mathematical fundamentals and concepts required for the subsequent chapters of this thesis. The chapter begins with a summary of the theory of vibrations, wave propagation and periodic medium, which is then followed by a literature survey of the available methods to analyze infinite periodic structures.

### 2.1 Fundamentals of vibration theory

#### 2.1.1 Free vibration of undamped systems

Mechanical vibration analysis plays a key role in predicting potential vibration problems in engineering designs. When problems are predicted, designs can be modified to mitigate vibration before systems are manufactured. In general, the mathematical tools for modeling potential vibration or acoustic problems make use of the free vibration properties. Free vibration can be defined as the oscillatory response of a mechanical system about an equilibrium position that occurs in the absence of an external excitation after having imposed an initial disturbance. The reason why mechanical systems vibrate freely is due to the exchange of energy between the system's inertial elements and elastic elements [Rixen 2017].

A mechanical system in free vibration oscillates with fixed frequencies known as natural frequencies. The patterns of motion in which all the components of the system move with these frequencies are called mode shapes, which in combination can represent any dynamic response of the system. Therefore, characterizing the mechanical system and finding its mode shapes provide essential information to represent intrinsically the system.

In general, a dynamic mechanical system without the consideration of damping can be analyzed by a discrete model with the following equation:

$$\mathbf{M}\ddot{\mathbf{q}} + \mathbf{K}\mathbf{q} = \mathbf{F} \quad (2.1)$$

where  $\mathbf{M}$ ,  $\mathbf{K}$ , and  $\mathbf{F}$  denote respectively the mass matrix of dimension  $p \times p$ , the stiffness matrix of dimension  $p \times p$ , and the load vector of dimension  $p \times 1$  which contains the externally applied loads. The  $p$  degrees of freedom that describe the system and their corresponding accelerations are respectively represented by the vectors  $\mathbf{q}$  and  $\ddot{\mathbf{q}}$ . If free vibration is considered, the equation 2.1 can be expressed as:

$$\mathbf{M}\ddot{\mathbf{q}} + \mathbf{K}\mathbf{q} = \mathbf{0} \quad (2.2)$$

Besides the trivial solution  $\mathbf{q} = \mathbf{0}$ , there are non-trivial solutions which represent the balance at every instant between the elastic and inertia forces. If an exponential approach with

$$\mathbf{q} = \Phi e^{i\omega t} \quad (2.3)$$

and

$$\ddot{\mathbf{q}} = -\omega^2 \Phi e^{i\omega t} \quad (2.4)$$

is considered, the system of equations 2.2 can be transformed into an homogenous linear system of equations representing the following matrix eigenvalue problem:

$$(\mathbf{K} - \omega^2 \mathbf{M})\Phi = \mathbf{0} \quad (2.5)$$

The non-trivial solutions for the displacements  $\mathbf{q}$  are then only possible if

$$\det(\mathbf{K} - \omega^2 \mathbf{M}) = 0 \quad (2.6)$$

The equation 2.6 leads to an equation for  $\omega$  with  $p$  eigenvalues or eigenfrequencies  $\omega_{Er}^2$ . By construction, the mass and stiffness matrices are symmetric and positive or semi-positive definite, meaning that the eigenvalues are always positive real numbers or zero. For each of these eigenvalues corresponds a solution of the equation system 2.5,  $\Phi_r$  of degree  $p$  called eigenmode or mode shape. The amplitude that represents each of these eigenmodes can be scaled arbitrary. In some cases, the mass matrix can be semi-positive definite if some degrees of freedom have no associated mass such as the case where there is a node in between two spring elements. On the other hand, the stiffness matrix is not positive definite, when the equilibrium position around which the oscillations are analyzed is not stable and if rigid body modes are present, indicating that no elastic forces (hence no deformations) are associated with the displacement of certain mode [Rixen 2017]. In general, the mass and stiffness matrices are semi-positive especially if they are determined with finite element method.

The mode shapes also possess a very important characteristic known as orthogonality with respect to the mass and stiffness matrix. This property can be written respectively as:

$$\Phi_s^T \mathbf{M} \Phi_r = A_r \delta_{rs} \quad (2.7)$$

and

$$\Phi_s^T \mathbf{K} \Phi_r = A_r \omega_r^2 \delta_{rs} \quad (2.8)$$

where  $\delta_{rs}$  is the Kronecker delta ( $\delta_{rs} = 1$  if  $r = s$ ,  $\delta_{rs} = 0$  if  $r \neq s$ ) and  $A_r$  is called the generalized mass of mode  $r$ . Since the mode shapes can be scaled arbitrarily, it is a common practice to normalize them in such a way that  $A_r = 1$ . Physically speaking, the orthogonality with respect to the mass matrix expresses that the work produced by the inertia forces of mode  $r$  on a displacement described by mode  $s$  is zero. Analogously, the orthogonality with respect to the stiffness matrix expresses that the work produced by the elastic forces of mode  $r$  on a displacement described by mode  $s$  is zero [Rixen 2017].

## 2.1.2 Description of damping in discrete systems

All real-life structures possess some kind of damping or energy dissipation mechanism when they vibrate. The specific ways in which energy is dissipated due to vibration depend on the specific numerous physical mechanisms that are operating throughout the system. The various damping mechanisms can be examined through its effect on a damped system in free vibration. In general, the equations of motion can be expressed by:

$$\mathbf{M} \ddot{\mathbf{q}} + \mathbf{C} \dot{\mathbf{q}} + \mathbf{K} \mathbf{q} = \mathbf{0} \quad (2.9)$$

where  $\mathbf{C}$  denotes the damping matrix. One of the most common hypotheses to characterize the damping is the proportional damping or also called Rayleigh damping, which is a way to build a damping matrix as a linear combination of  $\mathbf{M}$  and  $\mathbf{K}$  as follows:

$$\mathbf{C} = \alpha \mathbf{M} + \beta \mathbf{K} \quad (2.10)$$

where  $\alpha$  and  $\beta$  are predefined real constants that fit the measured data of the modal damping ratio  $\zeta_r$  for two modes at different frequencies as follows:

$$\zeta_r = \frac{1}{2} \left( \frac{\alpha}{\omega_r} + \beta \omega_r \right) \quad (2.11)$$

where all other modal damping ratios are determined but do in general over- or underestimate the real ones [Govers 2015].

If the values of  $\alpha$  and  $\beta$  are calculated for a specific constant modal damping ratio  $\zeta$  over a range of frequency, two equations can be solved:

$$\alpha = 2\zeta \frac{\omega_1 \omega_2}{\omega_1 + \omega_2} \quad (2.12)$$

and

$$\beta = \frac{2\zeta}{\omega_1 + \omega_2} \quad (2.13)$$

In general, this damping model assumes that in the system the damping forces are distributed partly like the elastic forces and partly like the inertia forces. However, physically speaking there is no reason for that assumption and its construction is used for convenience when it comes to get diagonal matrices [Rixen 2017]. Additionally, if the spatial distribution of the damping differs significantly from the distribution of mass or stiffness, this is when there are discrete damping elements like tuned mass dampers, the Rayleigh approach is not applicable any more [Buchsenschmid 2017].

### 2.1.3 Tuned mass dampers

A Tuned Mass Damper (TMD) is a passive control system used to reduce significantly the amplitude of vibrations in mechanical systems. The TMD is mounted in the primary structure and tuned to a certain eigenfrequency so that when it reaches that eigenfrequency a large amount of the structural vibrating energy is transferred to the TMD and then dissipated by a damping element as the primary structure is subjected to external loads. A properly tuning leads to excellent reductions of vibrations for loads applied at the resonant frequency but it is less effective for loads applied at different frequencies.

Basically, a TMD consists of three elements: mass, stiffness, and damping. The effectiveness of it relies on a proper choice of its location, the mass and a proper tuning of the stiffness and damping according to the previous identification of the eigenmodes of the main system and the TMD. The damping is chosen to optimize the energy dissipation over the bandwidth of the TMD, the stiffness and mass are selected to provide a TMD with the resonance frequency very close to the structure's resonance frequency and also with the desired level of vibration mitigation [Sims 2007].

### 2.1.4 Basic concepts of structural waves

A mechanical wave is a periodic disturbance that moves through a medium. Periodic waves are characterized by their frequency  $f$  or circular frequency  $\omega$ , speed of propagation  $v$ , and wavelength  $\lambda$ . In general,  $v$  depends on the physical properties of the wave medium. The wavelength is the distance along the direction of propagation over which the wave's shape repeats. The relationship between the speed of the wave, the wavelength and the frequency can be written as:

$$v = \lambda f \quad (2.14)$$

Another important parameter in wave description of vibrations is the wave number  $\kappa$ , which is the number of complete harmonic oscillations per unit distance and it is given by the following expression:

$$\kappa = \frac{2\pi}{\lambda} \quad (2.15)$$

The equation that relates the wave number to the angular frequency and describes how the speed of waves varies at different wavelengths, is called dispersion relation, and it is given by:

$$v = \frac{\omega}{\kappa} \quad (2.16)$$

Dispersion can be defined as the phenomenon where for different wave numbers, each harmonic component that comprises the wave propagates at its own velocity, causing a change of the wave's shape [Manconi 2008]. However, if all wavelengths travel at the same speed, that is  $v$  is independent of  $\kappa$ , the waves are non-dispersive, and the shape of the wave will remain the same.

There are three basic types of mechanical waves: longitudinal waves, shear waves, and bending or also known as flexural waves. In the longitudinal waves the particles of the medium move in the same direction as the wave propagation whereas in shear waves the particles of the medium move perpendicular to the wave propagation. For most practical structures, one or two geometric dimensions are small with respect to the wavelength. Under this assumption, the speed of a longitudinal wave is determined by the Young's modulus  $E$  and the density  $\rho$  of the medium according to:

$$v_l = \sqrt{\frac{E}{\rho}} \quad (2.17)$$

When a shear wave takes place the wave speed is governed by the shear modulus  $G$ , which depends on the Young's modulus  $E$  and the Poisson's ratio  $\nu$ , as follows:

$$v_s = \sqrt{\frac{G}{\rho}} \quad (2.18)$$

where

$$G = \frac{E}{2(1 + \nu)} \quad (2.19)$$

Due to the fact that the shear modulus is less than the Young's modulus, the shear waves are slower than longitudinal waves.

On the other hand, a bending wave is considered a hybrid between the longitudinal wave and the shear wave where the solid medium undergoes compressional and extensional deformations. Furthermore, bending waves are dispersive, meaning that the waves at low frequencies travel slower than waves at higher frequencies and the shape of the wave will therefore be distorted. This can be seen in the equation of speed for thin beams and plates where the wave speed depends on the frequency.

The wave speed for bending in thin beams is expressed by:

$$v_b = \sqrt[4]{\frac{EI\omega^2}{\rho A}} \quad (2.20)$$

where  $A$  is the cross-sectional area and  $I$  the second moment of inertia.

For the case of thin plates the equation for the bending wave speed is the following:

$$v_p = \sqrt[4]{\frac{D\omega^2}{\rho h}} \quad (2.21)$$

where  $h$  is the thickness of the plate and  $D$  is the flexural rigidity defined by:

$$D = \frac{Eh^3}{12(1 - \nu^2)} \quad (2.22)$$

The speed of a bending wave depends not only on the elastic moduli and density of the structural medium, but also on its geometric properties of the beam or the plate in question. However, the critical condition to deal with this kind of waves is that the cross section of the beam or plate remains rigid during the wave propagation [Manconi 2008].

## 2.2 Periodic structures

### 2.2.1 Potential of periodic structures in engineering

A periodic structure can be defined as a structure that is assembled by identical elements, called unit-cells, which are coupled to each other along one or more directions, as it is shown in figure 2.1.

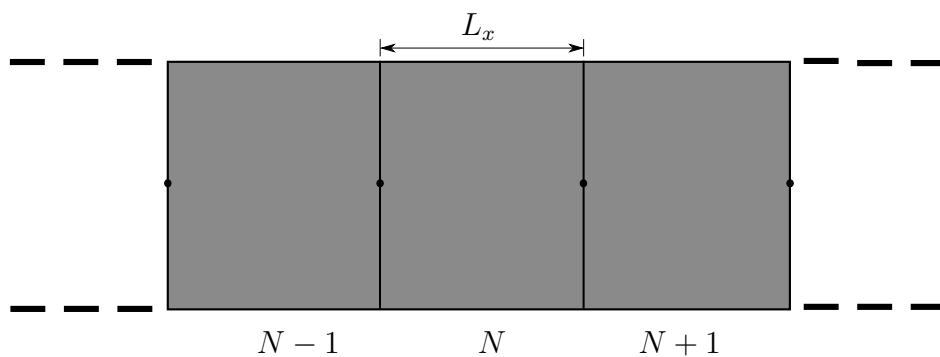


**Figure 2.1:** Periodic structure as an assembly of identical unit-cells of length  $L_x$

Nowadays, the application of these structures are observed on many engineering systems due to their numerous advantages such as improved material properties and dynamic behavior, characteristics that are useful in waveguides and filters. However, the ideas about the application of periodicity were first conceived in solid physics [Farzbod 2010].

In the early years of quantum mechanics, Felix Bloch formulated the concept of electron bands in crystals, developing the term band theory. Around 1990, the understanding of periodicity in material crystals led to a high number of applications in solid state physics, such as phononic crystals which showed attenuation of elastic waves in certain frequency bands. Further research was performed to transfer these concepts to elastodynamics resulting in attractive materials with excellent mechanical properties, simplification of its dynamical analysis by the analysis of one single unit-cell and the ability to reduce as well as to mitigate the noise transmission and vibrations [Hussein 2006].

In general, for the improvement of vibro-acoustic attenuation exist conventional methods, which rely on the addition of absorptive layers that leads to get heavy materials and unsatisfactory improvement of the low-frequency vibro-acoustic response of lightweight applications. This is because in order to be efficient, the thickness of the absorptive layer should be in the same order of magnitude as the acoustic wave length [Claeys 2013]. On the other hand,

there is another method which improves vibro-acoustic attenuation by the application of band theory. The basic principle is the interference of propagating waves on the unit-cell level such that there are zones with no free wave propagation in a frequency range, known as stop bands. In case where the waves can propagate, energy will be transmitted and pass bands are exhibited [Claeys 2013] [Brillouin 1953].

In general, there are two mechanisms that lead to stop bands, Bragg scattering and local resonance. The Bragg scattering stop band relies on periodicity, so that there are zones with destructive interference within the unit-cell, making smaller the amplitude of the original wave. On the other hand, the local resonance stop band depends on the properties of local resonators, but not on the period length. The stop band gap can also be partial where waves can not propagate in certain directions within a frequency range [Ruzzene 2010].

## 2.2.2 Methods of analysis for periodic structures

From the time of Isaac Newton up to now the ideas of free wave propagation in periodic structures have been developed. Rayleigh was the first to study a continuous periodic structure in 1887 which is applicable to any simple periodic structure with the wave motion governed by a second order differential equation [Mead 1995]. However, the formal mathematical basis was developed by the french mathematician Gaston Floquet, who proposed analytical solutions to ordinary differential equations with periodic coefficients [Silva 2015].

Due to the increasing need to analyze complicated crystal lattice structures in solid physics, more sophisticated mathematical techniques were developed between 1900 and 1960. One of them was developed by Felix Bloch, which was based on the mathematical work of Floquet. He proposed the theory to convert the study of a whole periodic structure into the study of a single unit-cell. Methods based on the Bloch theory have since been adapted to study elastic wave propagation in periodic structures and have been useful for both the physicist, who study wave phenomena taking place in microscopic periodic medium, and engineers, who are primarily interested in the wave characteristics of macroscopic periodic engineering structures such as railway tracks, acoustical ducts, car tires, etc [Farzbod 2010].

Another pioneering works were made by [Mead 1995] in the University of Southampton who proposed the general theory of wave propagation for periodic structures, making contributions to the analysis of free and forced wave motion in continuous periodic structures, and also provided an early discussion of damping in a one-dimensional infinite periodic structure. In early age of his research, he developed the receptance method, which was mainly used to

calculate propagation in periodic simply supported beam and plate stiffened periodically in one direction. Later, he and his colleges developed several numerical approaches which take advantage of the structure periodicity. In fact, these methods in general make use of Bloch's theory and they are regarded as the starting point for the development of a wave-based numerical method for periodic structures [Mead 1995].

Lin and McDaniel in 1969 were pioneers of the proposition of the Transfer Matrix Method (TMM) to the analysis of stiffened plate vibration and periodic structures. In the method, the generalized displacement and forces at the left-hand end and right-hand end of one periodic element are combined into state vectors. The state vectors at two ends are related through the periodic transfer matrix. However, due to the ill-conditioning of the problem Zhong in 1994 proposed a new formulation in terms of  $(\mu + 1/\mu)$  of the eigenvalue problem to overcome the numerical problems of the ill-conditioning using the symplectic property of transfer matrices [Zhong 1995].

Orris and Petyt in 1974 introduced the finite element method in the transfer matrix method to calculate the propagation constants in a one-dimensional periodic structure. The method is called Wave Finite Element Method (WFEM). A period of the structure is modeled using conventional finite element methods and thus the equation of motion for time-harmonic motion is obtained in terms of a discrete number of nodal degrees of freedom and forces. The boundary conditions are then applied and an eigenvalue problem is obtained whose solutions lead to the dispersion curves and wave modes.

Later, the WFEM was successfully applied to study the dynamic behavior in two-dimensional structures for low and mid frequency [Manconi 2008]. Additionally, [Zhou 2014] proposed a wave and modal coupled approach to study the wave propagation in periodic structures. The method is known as Condensed Wave Finite Element Method (CWFEM), and it enables to analyze the local behavior of the unit-cell using a reduced modal basis. For reasons of brevity most of the works are not cited here but the reader can find many references in [Mead 1995], [Sohir 2017] or [Silva 2015].

## 2.3 One-dimensional wave finite element method

The wave finite element method has been used to study the low-to-mid frequency wave motion in homogeneous periodic structures [Manconi 2008]. It is based on the periodic structure theory developed by [Mead 1995] from the Bloch's theory, meaning that the study of the whole periodic structure can be performed through the analysis of one unit-cell.

The method proposes an approach which combines the analytical theory for wave propagation in periodic structures with the capabilities of commercial finite element software. The unit-cell is modeled using conventional finite elements. The resulting mass, damping, and stiffness matrices are then post-processed to formulate the dynamic stiffness matrix of the unit-cell. Subsequently, periodic structure theory is applied in order to obtain an eigenproblem whose solutions provide the description of the wave propagation characteristics [Manconi 2008].

### 2.3.1 Floquet's theorem

In 1883 Floquet transformed a periodic system into a linear system of equations by giving a canonical form to the matrix solutions of the system. He demonstrated that a time harmonic electromagnetic field at a point in an infinite one-dimensional periodic structure varies  $e^k$  with respect to the field at the corresponding point in the preceding unit-cell [Bostani 2012].

The Floquet's theorem can then be expressed mathematically as:

$$V(x + L_x) = V(x)e^k = V(x)e^{-i\kappa L_x} \quad (2.23)$$

where  $V(x)$  is a periodic function with period  $L_x$ ,  $k = -i\kappa L_x$  is the propagation constant, and  $\kappa = -\kappa_R - i\kappa_I$  is the Floquet wave number where the real and imaginary parts determine respectively the phase and the attenuation per unit length. The amplitude of free response  $V(x)$  is a spatially dependent wave amplitude that is periodic with the same period as the structure, and it is a function of the frequency of oscillation [Bostani 2012].

When periodic boundary conditions are applied, the master and slave boundaries can be defined according to the direction of the wave propagation, as figure 2.2 shows. The master boundary is coupled with the slave boundary such that the complex propagation constant (phase shift and attenuation from the master boundary) fulfills the Floquet's principle.

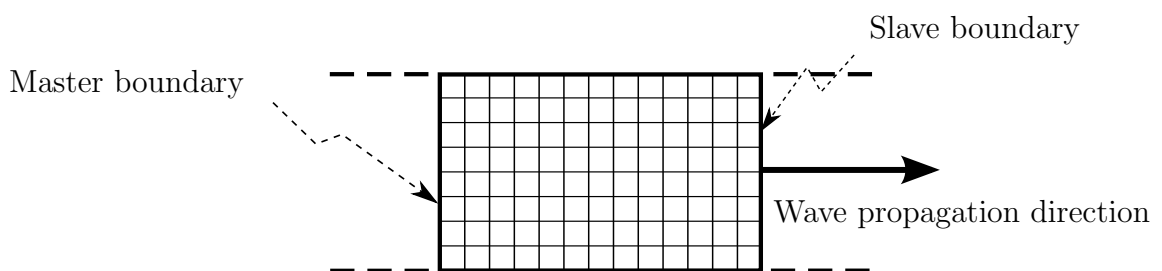


**Figure 2.2:** Floquet's boundary definition in a unit-cell

### 2.3.2 Unit-cell dynamics

For the dynamic equilibrium formulation of a periodic elastic structure, an assembly of an infinite number of unit-cells is considered along the direction of the wave propagation. However, in order to predict the characteristics of wave motion for harmonic motion at frequency  $\omega$ , only one unit-cell is enough to model by conventional finite element analysis, so that the dynamic equilibrium equation is expressed in the frequency domain as:

$$\mathbf{D}\mathbf{q} = \mathbf{F} \quad (2.24)$$

where  $\mathbf{q}$  and  $\mathbf{F}$  are respectively vectors of nodal displacements/rotations and forces/momenta, and  $\mathbf{D}$  is the dynamic stiffness matrix defined as:

$$\mathbf{D} = -\omega^2 \mathbf{M} + i\omega \mathbf{C} + \mathbf{K} \quad (2.25)$$

The extraction of  $\mathbf{M}$ ,  $\mathbf{C}$  and  $\mathbf{K}$  can be performed with the help of any commercial finite element package. As a remark, depending on the assumptions of the problem, the damping may be modeled by Rayleigh damping. However, if damping is neglected from the system, the equation of motion will be given by:

$$(-\omega^2 \mathbf{M} + \mathbf{K})\mathbf{q} = \mathbf{F} \quad (2.26)$$

The equation 2.26 can be solved with two different well-known approaches depending on the type of solution to be sought. The direct approach, which computes the wave number for a certain value of frequency, and the inverse approach, which derives the dispersion properties for a certain value of the wave number [Claeys 2013].

### 2.3.3 Direct approach

In the direct approach the frequency in equation 2.26 is known. If free wave propagation is considered, the effect of external forces is not taken into account. The only forces acting on the unit-cell are the ones on its boundaries caused by its adjacent unit-cells. Therefore, the dynamic stiffness matrix can be partitioned and the equation of motion can be rewritten in general as follows:

$$\begin{bmatrix} \mathbf{D}_{BB} & \mathbf{D}_{BI} \\ \mathbf{D}_{IB} & \mathbf{D}_{II} \end{bmatrix} \begin{bmatrix} \mathbf{q}_B \\ \mathbf{q}_I \end{bmatrix} = \begin{bmatrix} \mathbf{f}_B \\ \mathbf{0} \end{bmatrix} \quad (2.27)$$

where the subscripts  $B$  and  $I$  make reference to the boundary nodes and to the interior nodes respectively. Therefore,  $\mathbf{q}_B$  and  $\mathbf{q}_I$  are respectively the vector of displacement/rotations of the boundary nodes and internal nodes whereas the vector of force/moment of the boundary nodes is denoted by  $\mathbf{f}_B$ . Additionally, from the second line of 2.27 it follows that the interior degrees of freedom can be given by:

$$\mathbf{q}_I = -\mathbf{D}_{II}^{-1}\mathbf{D}_{IB}\mathbf{q}_B \quad (2.28)$$

The equation 2.28 eliminates the interior degrees of freedom, leading to the expression of the condensed dynamic matrix  $\mathbf{D}_C$  as follows:

$$\mathbf{D}_C\mathbf{q}_B = \mathbf{f}_B \quad (2.29)$$

with

$$\mathbf{D}_C = \mathbf{D}_{BB} - \mathbf{D}_{BI}\mathbf{D}_{II}^{-1}\mathbf{D}_{IB} \quad (2.30)$$

According to [Mace 2005] for one-dimensional propagation, it can be defined two boundaries, one left-hand boundary and one right-hand boundary as it is shown in figure 2.3.

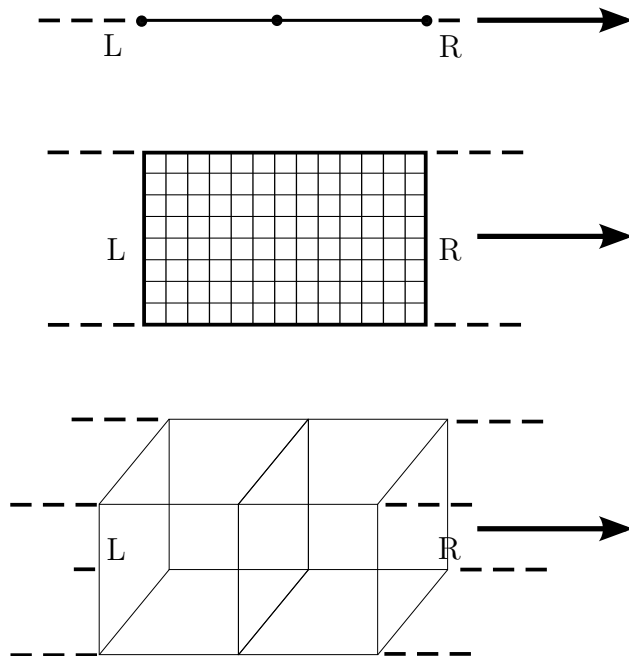


**Figure 2.3:** One-, two- and three-dimensional unit-cell models with their respective left and right boundary under one-dimensional wave propagation.

As a result, the dynamic stiffness matrix can be partitioned in the following way:

$$\mathbf{D} = \begin{bmatrix} \mathbf{D}_{LL} & \mathbf{D}_{LR} & \mathbf{D}_{LI} \\ \mathbf{D}_{RL} & \mathbf{D}_{RR} & \mathbf{D}_{RI} \\ \mathbf{D}_{IL} & \mathbf{D}_{IR} & \mathbf{D}_{II} \end{bmatrix} \quad (2.31)$$

where the subscripts  $R$ ,  $L$  and  $I$  are respectively related to the set of degrees of freedom of the nodes on the right and left cross section as well as of the interior nodes of the unit-cell. Substituting equation 2.31 in equation 2.24 and considering the degrees of freedom of the model of a unit-cell on the left side, right side and the internal ones as well as no external forces on the internal nodes yield to:

$$\begin{bmatrix} \mathbf{D}_{LL} & \mathbf{D}_{LR} & \mathbf{D}_{LI} \\ \mathbf{D}_{RL} & \mathbf{D}_{RR} & \mathbf{D}_{RI} \\ \mathbf{D}_{IL} & \mathbf{D}_{IR} & \mathbf{D}_{II} \end{bmatrix} \begin{bmatrix} \mathbf{q}_L \\ \mathbf{q}_R \\ \mathbf{q}_I \end{bmatrix} = \begin{bmatrix} \mathbf{f}_L \\ \mathbf{f}_R \\ \mathbf{0} \end{bmatrix} \quad (2.32)$$

From the third line of equation 2.32, the interior degrees of freedom can be expressed by:

$$\mathbf{q}_I = -\mathbf{D}_{II}^{-1}(\mathbf{D}_{IL}\mathbf{q}_L + \mathbf{D}_{IR}\mathbf{q}_R) \quad (2.33)$$

Eliminating the internal degrees of freedom from equation 2.32 leads to the definition of the condensed dynamic matrix as follows:

$$\mathbf{D}_C = \begin{bmatrix} \tilde{\mathbf{D}}_{LL} & \tilde{\mathbf{D}}_{LR} \\ \tilde{\mathbf{D}}_{RL} & \tilde{\mathbf{D}}_{RR} \end{bmatrix} \quad (2.34)$$

With help of equation 2.34, the equation of motion can be rewritten as:

$$\begin{bmatrix} \tilde{\mathbf{D}}_{LL} & \tilde{\mathbf{D}}_{LR} \\ \tilde{\mathbf{D}}_{RL} & \tilde{\mathbf{D}}_{RR} \end{bmatrix} \begin{bmatrix} \mathbf{q}_L \\ \mathbf{q}_R \end{bmatrix} = \begin{bmatrix} \mathbf{f}_L \\ \mathbf{f}_R \end{bmatrix} \quad (2.35)$$

where the blocks  $\tilde{\mathbf{D}}_{LL}$ ,  $\tilde{\mathbf{D}}_{LR}$ ,  $\tilde{\mathbf{D}}_{RL}$  and  $\tilde{\mathbf{D}}_{RR}$  are:

$$\tilde{\mathbf{D}}_{LL} = \mathbf{D}_{LL} - \mathbf{D}_{LI}\mathbf{D}_{II}^{-1}\mathbf{D}_{IL} \quad (2.36a)$$

$$\tilde{\mathbf{D}}_{RL} = \mathbf{D}_{RL} - \mathbf{D}_{RI}\mathbf{D}_{II}^{-1}\mathbf{D}_{IL} \quad (2.36b)$$

$$\tilde{\mathbf{D}}_{LR} = \mathbf{D}_{LR} - \mathbf{D}_{LI}\mathbf{D}_{II}^{-1}\mathbf{D}_{IR} \quad (2.36c)$$

$$\tilde{\mathbf{D}}_{RR} = \mathbf{D}_{RR} - \mathbf{D}_{RI}\mathbf{D}_{II}^{-1}\mathbf{D}_{IR} \quad (2.36d)$$

Due to the symmetry of the dynamic stiffness matrix, the following relations are valid:

$$\tilde{\mathbf{D}}_{LL}^T = \tilde{\mathbf{D}}_{LL} \quad (2.37a)$$

$$\tilde{\mathbf{D}}_{RR}^T = \tilde{\mathbf{D}}_{RR} \quad (2.37b)$$

$$\tilde{\mathbf{D}}_{LR}^T = \tilde{\mathbf{D}}_{RL} \quad (2.37c)$$

The analysis considers the interaction of cross sections of successive unit-cells as shown in the figure 2.4. When no external forces are applied on the structure as well as continuity of displacements and equilibrium of forces at the boundary are considered, the displacements and forces of the nodes on the right boundary of the unit-cell number  $N$  are related with the displacements and forces of the left boundary of the successive unit-cell number  $N + 1$  as follows:

$$\mathbf{q}_R^N = \mathbf{q}_L^{N+1} \quad (2.38a)$$

$$\mathbf{f}_R^N = -\mathbf{f}_L^{N+1} \quad (2.38b)$$

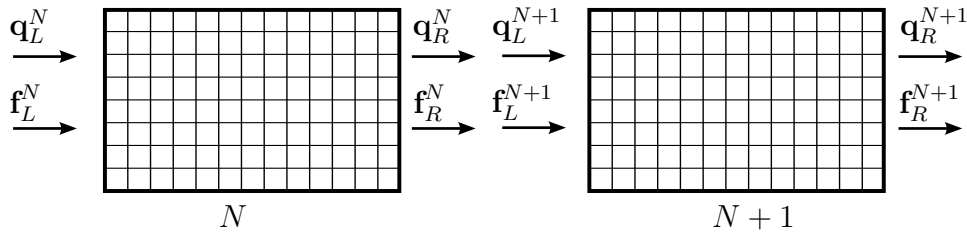


**Figure 2.4:** Interaction between two unit-cells

The set of conditions given by 2.38a and 2.38b as well as the equation 2.35 yield to define the transfer matrix as:

$$\mathbf{T} = \begin{bmatrix} -\tilde{\mathbf{D}}_{LR}^{-1}\tilde{\mathbf{D}}_{LL} & \tilde{\mathbf{D}}_{LR}^{-1} \\ -\tilde{\mathbf{D}}_{RL} + \tilde{\mathbf{D}}_{RR}\tilde{\mathbf{D}}_{LR}^{-1}\tilde{\mathbf{D}}_{LL} & -\tilde{\mathbf{D}}_{RR}\tilde{\mathbf{D}}_{LR}^{-1} \end{bmatrix} \quad (2.39)$$

which yields to formulate the following set of equations:

$$\begin{bmatrix} \mathbf{q}_L \\ \mathbf{f}_L \end{bmatrix}_{N+1} = \mathbf{T} \begin{bmatrix} \mathbf{q}_L \\ \mathbf{f}_L \end{bmatrix}_N \quad (2.40)$$

From the Floquet's theorem, the force/moment vector and displacements/rotations vector

are related along the waveguide by the following expression:

$$\begin{bmatrix} \mathbf{q}_R \\ \mathbf{f}_R \end{bmatrix}_N = \begin{bmatrix} \mathbf{q}_L \\ \mathbf{f}_L \end{bmatrix}_{N+1} = \mu \begin{bmatrix} \mathbf{q}_L \\ \mathbf{f}_L \end{bmatrix}_N \quad (2.41)$$

which leads to describe the wave propagation through the following eigenvalue problem:

$$\mathbf{T} \begin{bmatrix} \mathbf{q}_L \\ \mathbf{f}_L \end{bmatrix}_N = \mu \begin{bmatrix} \mathbf{q}_L \\ \mathbf{f}_L \end{bmatrix}_N \quad (2.42)$$

The equation 2.42 yields to  $n$  pairs of eigenvalues  $(\mu, 1/\mu)$  or wave numbers  $(\kappa, -\kappa)$ , and their respective mode shapes, with  $n$  corresponding to the number of degrees of freedom in the cross section of the analyzed boundary [Mace 2005]. From the eigenvalues of  $\mathbf{T}$ , the propagation constants of the waves can be found as follows:

$$\mu = e^{-i\kappa L_x} = e^{-i(-\kappa_R - i\kappa_I)L_x} = e^{-\kappa_I L_x} e^{i\kappa_R L_x} = e^{-k_R + ik_I} \quad (2.43)$$

where  $\kappa_R$  and  $\kappa_I$  are respectively the change in phase and the attenuation per unit length. If  $|\mu| < 1$  the waves travel in the positive direction and if  $|\mu| > 1$  the waves travel in the negative direction. If no damping is assumed, the amplitude of propagating waves remain constant, with  $|\mu| = 1$ . These relations can be summarized in the table 2.1 and in figure 2.5, so that it is possible to plot and interpret the dispersion curves [Sohir 2017].

$ \mu $	$\kappa_R$	$\kappa_I$	Direction	Wave type
1	0	> 0	positive	propagating
< 1	>0	0	positive	evanescent
< 1	>0	> 0	positive	attenuating
1	0	< 0	negative	propagating
> 1	<0	0	negative	evanescent
> 1	<0	< 0	negative	attenuating

**Table 2.1:** Wave classification

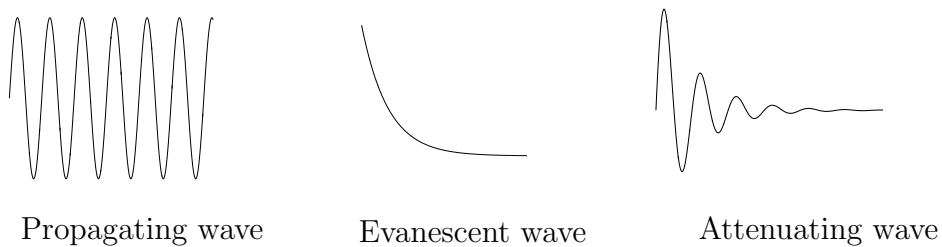


**Figure 2.5:** Type of waves in positive direction

The wave propagation mode shapes can be partitioned into  $n \times 1$  vectors associated with the degrees of freedom and forces on each node of the analyzed cross section as follows:

$$\Phi_k = \begin{bmatrix} \phi_k^q \\ \phi_k^f \end{bmatrix} \quad (2.44)$$

For models with high number of degrees of freedom, the transfer matrix  $\mathbf{T}$  may be ill-conditioned. To cope with that, there are some techniques that have been proposed.

### 2.3.4 LR method

The traditional WFEM is based on the transfer matrix  $\mathbf{T}$ . However, the computational cost is high due to the matrix inversions that have to be performed. Another formulation of the eigenvalue problem which has been used to reduce the computational cost is given by:

$$\mathbf{L} \begin{bmatrix} \mathbf{q}_L \\ \tilde{\mathbf{q}}_L \end{bmatrix} = \mu \mathbf{R} \begin{bmatrix} \mathbf{q}_L \\ \tilde{\mathbf{q}}_L \end{bmatrix} \quad (2.45)$$

where  $\tilde{\mathbf{q}}_L = \mu \mathbf{q}_L$  and  $\mathbf{L}$  and  $\mathbf{R}$  are given by:

$$\mathbf{L} = \begin{bmatrix} \mathbf{Z} & \tilde{\mathbf{D}}_{RL} \\ -\tilde{\mathbf{D}}_{RL} & -\tilde{\mathbf{D}}_{LL} - \tilde{\mathbf{D}}_{RR} \end{bmatrix} \quad (2.46)$$

and

$$\mathbf{R} = \begin{bmatrix} \tilde{\mathbf{D}}_{RL} & \mathbf{Z} \\ \mathbf{Z} & \tilde{\mathbf{D}}_{LR} \end{bmatrix} \quad (2.47)$$

The matrix  $\mathbf{Z}$  is the corresponding zero matrix [Silva 2015].

### 2.3.5 Zhong's method

Another important formulation of the eigenvalue problem, which overcome ill-conditioning, was proposed by [Zhong 1995]. He showed that the transfer matrix  $\mathbf{T}$  is symplectic, meaning that the eigenvalue problem can be defined in terms of  $(\mu + 1/\mu)$  as follows:

$$\begin{bmatrix} \tilde{\mathbf{D}}_{RL} & \mathbf{Z} \\ \mathbf{Z} & \tilde{\mathbf{D}}_{LR} \end{bmatrix} \begin{bmatrix} \mathbf{q}_L \\ \tilde{\mathbf{q}}_L \end{bmatrix} = \frac{1}{\mu + 1/\mu} \begin{bmatrix} -(\tilde{\mathbf{D}}_{RR} + \tilde{\mathbf{D}}_{LL}) & -(\tilde{\mathbf{D}}_{LR} - \tilde{\mathbf{D}}_{RL}) \\ (\tilde{\mathbf{D}}_{LR} - \tilde{\mathbf{D}}_{RL}) & -(\tilde{\mathbf{D}}_{RR} + \tilde{\mathbf{D}}_{LL}) \end{bmatrix} \begin{bmatrix} \mathbf{q}_L \\ \tilde{\mathbf{q}}_L \end{bmatrix} \quad (2.48)$$

According to [Zhong 1995] and [Silva 2015], this method leads to double eigenvalues in the form of  $\lambda_k = (\mu_k + 1/\mu_k)$ . The eigenvalues  $\mu$  can then be retrieved in the following way:

$$\mu_k = \frac{1}{2} \pm \sqrt{\lambda_k^2 - 4} \quad (2.49)$$

### 2.3.6 Condensed wave finite element method

One of the most effective methods to reduce the computational effort of complex one-dimensional waveguides models and to calculate the dispersion curves is the Condensed Wave Finite Element Method (CWFEM) proposed by [Zhou 2014].

The first step of the method is to obtain the partitions of the mass and stiffness matrices, so that the system of equations is given by:

$$\left( -\omega^2 \begin{bmatrix} \mathbf{M}_{LL} & \mathbf{M}_{LR} & \mathbf{M}_{LI} \\ \mathbf{M}_{RL} & \mathbf{M}_{RR} & \mathbf{M}_{RI} \\ \mathbf{M}_{IL} & \mathbf{M}_{IR} & \mathbf{M}_{II} \end{bmatrix} + \begin{bmatrix} \mathbf{K}_{LL} & \mathbf{K}_{LR} & \mathbf{K}_{LI} \\ \mathbf{K}_{RL} & \mathbf{K}_{RR} & \mathbf{K}_{RI} \\ \mathbf{K}_{IL} & \mathbf{K}_{IR} & \mathbf{K}_{II} \end{bmatrix} \right) \begin{bmatrix} \mathbf{q}_L \\ \mathbf{q}_R \\ \mathbf{q}_I \end{bmatrix} = \begin{bmatrix} \mathbf{f}_L \\ \mathbf{f}_R \\ \mathbf{0} \end{bmatrix} \quad (2.50)$$

The basic idea of [Zhou 2014] is to reformulate the physical internal degrees of freedom  $\mathbf{q}_I$  to a reduced modal basis of modal degrees of freedom with hybrid coordinates  $\mathbf{q}_H$ . This hybrid coordinates are related to the physical coordinates through the matrix  $\Theta$  as follows:

$$\begin{bmatrix} \mathbf{q}_L \\ \mathbf{q}_R \\ \mathbf{q}_I \end{bmatrix} = \Theta \begin{bmatrix} \mathbf{q}_L \\ \mathbf{q}_R \\ \mathbf{q}_H \end{bmatrix} \quad (2.51)$$

where  $\Theta$  is given by:

$$\Theta = \begin{bmatrix} \mathbf{I} & \mathbf{Z} & \mathbf{Z} \\ \mathbf{Z} & \mathbf{I} & \mathbf{Z} \\ \Psi_L & \Psi_R & \Psi_H \end{bmatrix} \quad (2.52)$$

where  $\Psi_L$  and  $\Psi_R$  are given by:

$$\Psi_L = -\mathbf{K}_{II}^{-1} \mathbf{K}_{IL} \quad (2.53)$$

and

$$\Psi_R = -\mathbf{K}_{II}^{-1} \mathbf{K}_{IR} \quad (2.54)$$

In order to get  $\Psi_H$ , first the so-called fixed interface modes  $\Psi_I$  have to be found. Making  $\mathbf{q}_L = \mathbf{q}_R = \mathbf{0}$  in equation 2.50 yields to the following eigenproblem:

$$(\mathbf{K}_{II} - \omega^2 \mathbf{M}_{II}) \Psi_I = \mathbf{0} \quad (2.55)$$

A reduced basis of  $\Psi_I$  is  $\Psi_H$  with  $m_H$  number of rows, corresponding to the number of rows of  $\Psi_I$ , and  $n_H$  number of columns whose selection corresponds to certain convergence criteria discussed by [Zhou 2014]. By the last step, the equation of motion 2.50 assuming time harmonic wave propagation can be reduced and rewritten in the following form:

$$\left( -\omega^2 \begin{bmatrix} \mathbf{M}_{LL}^* & \mathbf{M}_{LR}^* & \mathbf{M}_{LH}^* \\ \mathbf{M}_{RL}^* & \mathbf{M}_{RR}^* & \mathbf{M}_{RH}^* \\ \mathbf{M}_{HL}^* & \mathbf{M}_{HR}^* & \mathbf{M}_{HH}^* \end{bmatrix} + \begin{bmatrix} \mathbf{K}_{LL}^* & \mathbf{K}_{LR}^* & \mathbf{K}_{LH}^* \\ \mathbf{K}_{RL}^* & \mathbf{K}_{RR}^* & \mathbf{K}_{RH}^* \\ \mathbf{K}_{HL}^* & \mathbf{K}_{HR}^* & \mathbf{K}_{HH}^* \end{bmatrix} \right) \begin{bmatrix} \mathbf{q}_L \\ \mathbf{q}_R \\ \mathbf{q}_H \end{bmatrix} = \begin{bmatrix} \mathbf{f}_L \\ \mathbf{f}_R \\ \mathbf{0} \end{bmatrix} \quad (2.56)$$

where

$$\begin{bmatrix} \mathbf{M}_{LL}^* & \mathbf{M}_{LR}^* & \mathbf{M}_{LH}^* \\ \mathbf{M}_{RL}^* & \mathbf{M}_{RR}^* & \mathbf{M}_{RH}^* \\ \mathbf{M}_{HL}^* & \mathbf{M}_{HR}^* & \mathbf{M}_{HH}^* \end{bmatrix} = \Theta^T \begin{bmatrix} \mathbf{M}_{LL} & \mathbf{M}_{LR} & \mathbf{M}_{LI} \\ \mathbf{M}_{RL} & \mathbf{M}_{RR} & \mathbf{M}_{RI} \\ \mathbf{M}_{IL} & \mathbf{M}_{IR} & \mathbf{M}_{II} \end{bmatrix} \Theta \quad (2.57)$$

and

$$\begin{bmatrix} \mathbf{K}_{LL}^* & \mathbf{K}_{LR}^* & \mathbf{K}_{LH}^* \\ \mathbf{K}_{RL}^* & \mathbf{K}_{RR}^* & \mathbf{K}_{RH}^* \\ \mathbf{K}_{HL}^* & \mathbf{K}_{HR}^* & \mathbf{K}_{HH}^* \end{bmatrix} = \Theta^T \begin{bmatrix} \mathbf{K}_{LL} & \mathbf{K}_{LR} & \mathbf{K}_{LI} \\ \mathbf{K}_{RL} & \mathbf{K}_{RR} & \mathbf{K}_{RI} \\ \mathbf{K}_{IL} & \mathbf{K}_{IR} & \mathbf{K}_{II} \end{bmatrix} \Theta \quad (2.58)$$

Leading to express the equation 2.32 as:

$$\begin{bmatrix} \mathbf{D}_{LL}^* & \mathbf{D}_{LR}^* & \mathbf{D}_{LH}^* \\ \mathbf{D}_{RL}^* & \mathbf{D}_{RR}^* & \mathbf{D}_{RH}^* \\ \mathbf{D}_{HL}^* & \mathbf{D}_{HR}^* & \mathbf{D}_{HH}^* \end{bmatrix} \begin{bmatrix} \mathbf{q}_L \\ \mathbf{q}_R \\ \mathbf{q}_H \end{bmatrix} = \begin{bmatrix} \mathbf{f}_L \\ \mathbf{f}_R \\ \mathbf{0} \end{bmatrix} \quad (2.59)$$

According to the formulation of [Mace 2005], the internal degrees of freedom can be removed through the dynamic condensation, having the same form as equation 2.35:

$$\begin{bmatrix} \tilde{\mathbf{D}}_{LL}^* & \tilde{\mathbf{D}}_{LR}^* \\ \tilde{\mathbf{D}}_{RL}^* & \tilde{\mathbf{D}}_{RR}^* \end{bmatrix} \begin{bmatrix} \mathbf{q}_L \\ \mathbf{q}_R \end{bmatrix} = \begin{bmatrix} \mathbf{f}_L \\ \mathbf{f}_R \end{bmatrix} \quad (2.60)$$

with

$$\tilde{\mathbf{D}}_{LL}^* = \mathbf{D}_{LL}^* - \mathbf{D}_{LH}^* (\mathbf{D}_{HH}^*)^{-1} \mathbf{D}_{HL}^* \quad (2.61a)$$

$$\tilde{\mathbf{D}}_{RL}^* = \mathbf{D}_{RL}^* - \mathbf{D}_{RH}^* (\mathbf{D}_{HH}^*)^{-1} \mathbf{D}_{HL}^* \quad (2.61b)$$

$$\tilde{\mathbf{D}}_{LR}^* = \mathbf{D}_{LR}^* - \mathbf{D}_{LH}^* (\mathbf{D}_{HH}^*)^{-1} \mathbf{D}_{HR}^* \quad (2.61c)$$

$$\tilde{\mathbf{D}}_{RR}^* = \mathbf{D}_{RR}^* - \mathbf{D}_{RH}^* (\mathbf{D}_{HH}^*)^{-1} \mathbf{D}_{HR}^* \quad (2.61d)$$

The complexity to invert  $\mathbf{D}_{HH}^*$  is less than the one of  $\mathbf{D}_{II}$ . Once the dynamic condensation of the internal degrees of freedom has been performed, the equation of motion of the unit-cell takes the form as in the classical WFEM, so that the eigenvalue problem is expressed by:

$$\hat{\mathbf{N}} \begin{bmatrix} \mathbf{q}_L \\ \mathbf{q}_R \end{bmatrix} = \mu \hat{\mathbf{L}} \begin{bmatrix} \mathbf{q}_L \\ \mathbf{q}_R \end{bmatrix} \quad (2.62)$$

where

$$\hat{\mathbf{N}} = \begin{bmatrix} \mathbf{Z} & \mathbf{I} \\ \tilde{\mathbf{D}}_{RL}^* & \tilde{\mathbf{D}}_{RR}^* \end{bmatrix} \quad (2.63)$$

and

$$\hat{\mathbf{L}} = \begin{bmatrix} \mathbf{I} & \mathbf{Z} \\ -\tilde{\mathbf{D}}_{LL}^* & -\tilde{\mathbf{D}}_{LR}^* \end{bmatrix} \quad (2.64)$$

Finally, the state vector composed by  $\mathbf{q}_L$  and  $-\mathbf{f}_L$  is given by:

$$\begin{bmatrix} \mathbf{q}_L \\ -\mathbf{f}_L \end{bmatrix} = \hat{\mathbf{L}} \begin{bmatrix} \mathbf{q}_L \\ \mathbf{q}_R \end{bmatrix} \quad (2.65)$$

### 2.3.7 Dispersion curves

To study the wave propagation characteristics in periodic structures, it is important to conduct an eigenvalue analysis of the unit-cell model. From this eigenvalue analysis, the characteristics of a wave propagation can be represented with the help of the frequency  $f$  and the propagation constants  $k$  in curves called dispersion curves [Claeys 2013]. In this way, the stop bands can be detected and physical insight of the dynamic behavior of periodic structures can be obtained.

The dispersion curve of each wave mode is obtained by analyzing the frequency evolution of the real and imaginary parts of the propagation constants. When the frequency is known, the real part  $k_R$  and imaginary part  $k_I$  can be extracted from the eigenvalues as follows:

$$k_R = -\ln |\mu| \quad (2.66)$$

and

$$k_I = \arctan \frac{\Im(\mu)}{\Re(\mu)} \quad (2.67)$$

If the frequency is not known, the inverse approach can be applied for certain range of wave numbers so that the so-called band structure can be obtained.

### 2.3.8 Inverse approach

The inverse approach aims to investigate how to manipulate the band gap frequencies for infinite undamped structures. It is assumed free wave propagation and the wave numbers are proposed, in a way such that the attenuation of the waves can not be predicted. Therefore, the propagation constant can be defined as:

$$\mu = e^{i\kappa_R L_x} \quad (2.68)$$

With compatible displacements and force balance at the boundaries of the unit-cell, a reduction matrix  $\mathbf{R}$  in terms of  $\mu$  can be derived such that:

$$\mathbf{R}^{*T}(-\omega^2 \mathbf{M} + \mathbf{K}) \mathbf{R} \mathbf{q}^{red} = \mathbf{R}^{*T} \mathbf{F} \quad (2.69)$$

where  $\mathbf{q}^{red}$  denotes the reduced displacements and  $*$  indicates the complex conjugate of the matrix [Claeys 2013]. If the internal forces are equal to zero, the reduced force vector  $\mathbf{R}^{*T} \mathbf{F}$  vanishes. Therefore, the equation of motion reduces to the following eigenvalue problem:

$$(-\omega^2 \mathbf{M}^{red} + \mathbf{K}^{red}) \mathbf{q}^{red} = \mathbf{0} \quad (2.70)$$

where  $\mathbf{M}^{red} = \mathbf{R}^{*T} \mathbf{M} \mathbf{R}$  and  $\mathbf{K}^{red} = \mathbf{R}^{*T} \mathbf{K} \mathbf{R}$  are the reduced mass and stiffness matrices respectively. Solving 2.70 for the frequency  $\omega$ , the frequencies of free wave propagation are found and if the propagation constants are imaginary, the matrix  $(-\omega^2 \mathbf{M}^{red} + \mathbf{K}^{red})$  is Hermitian and the solutions for  $\omega$  are always real [Claeys 2013].

According to the Floquet's theorem, the degrees of freedom and forces on the boundaries must be related in the following manner:

$$\mathbf{q}_R = \mu \mathbf{q}_L \quad (2.71a)$$

$$\mathbf{f}_R = \mu \mathbf{f}_L \quad (2.71b)$$

Using the above relations, the transformation matrix  $\mathbf{R}$  can be defined as follows:

$$\mathbf{R} = \begin{bmatrix} \mathbf{I} & \mathbf{Z} \\ \mathbf{Z} & \mathbf{I} \\ \mu\mathbf{I} & \mathbf{Z} \end{bmatrix} \quad (2.72)$$

which define:

$$\mathbf{q} = \begin{bmatrix} \mathbf{q}_L \\ \mathbf{q}_I \\ \mathbf{q}_R \end{bmatrix} = \begin{bmatrix} \mathbf{I} & \mathbf{Z} \\ \mathbf{Z} & \mathbf{I} \\ \mu\mathbf{I} & \mathbf{Z} \end{bmatrix} \begin{bmatrix} \mathbf{q}_L \\ \mathbf{q}_I \end{bmatrix} = \mathbf{R}\mathbf{q}^{red} \quad (2.73)$$

and for nodal forces:

$$\begin{bmatrix} \mathbf{I} & \mathbf{Z} & -\mu\mathbf{I} \\ \mathbf{Z} & \mathbf{I} & \mathbf{Z} \end{bmatrix} \begin{bmatrix} \mathbf{f}_L \\ \mathbf{0} \\ \mathbf{f}_R \end{bmatrix} = \mathbf{R}^{*T} \begin{bmatrix} \mathbf{f}_L \\ \mathbf{0} \\ \mathbf{f}_R \end{bmatrix} = \mathbf{0} \quad (2.74)$$

The system of equations 2.69 can be then rewritten for one-dimensional propagation as:

$$\mathbf{R}^{*T}(-\omega^2\mathbf{M} + \mathbf{K})\mathbf{R} \begin{bmatrix} \mathbf{q}_L \\ \mathbf{q}_I \end{bmatrix} = \mathbf{0} \quad (2.75)$$

Since  $\mu$  is proposed, the equation 2.75 becomes a standard eigenproblem of  $\omega^2$  given by:

$$(-\omega^2\mathbf{M}^{red} + \mathbf{K}^{red}) \begin{bmatrix} \mathbf{q}_L \\ \mathbf{q}_I \end{bmatrix} = \mathbf{0} \quad (2.76)$$

## 2.4 Two-dimensional wave finite element method

The purpose of this section is to extend the WFEM approach to two-dimensional undamped structures. Typically, this is performed in structures which can be assumed to be an assembly of rectangular segments of length  $L_x$  and  $L_y$  in  $x$  and  $y$  direction respectively.

The method includes the use of conventional finite element methods to obtain the equation of motion of the unit-cell. Periodic boundary conditions are then applied to relate the nodal degrees of freedom and forces. These degrees of freedom can be visualized in figure 2.6.

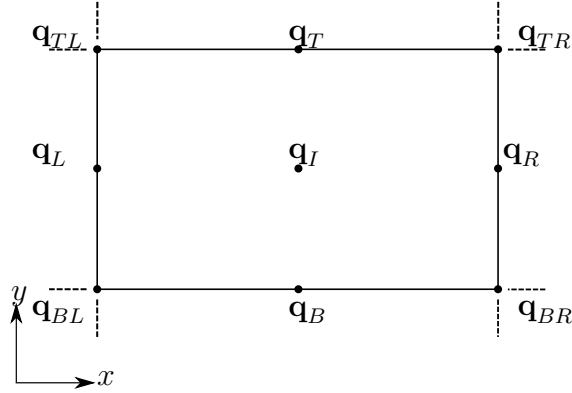


**Figure 2.6:** Two-dimensional unit-cell with its respective degrees of freedom

The edge nodes ( $\mathbf{q}_B, \mathbf{q}_T, \mathbf{q}_L, \mathbf{q}_R$ ), interior nodes  $\mathbf{q}_I$  and corner nodes ( $\mathbf{q}_{TL}, \mathbf{q}_{TR}, \mathbf{q}_{BL}, \mathbf{q}_{BR}$ ) can be arranged in the displacement/rotations vector  $\mathbf{q}$ , according to [Langley 1992], in the following way:

$$\mathbf{q} = [\mathbf{q}_L^T \quad \mathbf{q}_R^T \quad \mathbf{q}_B^T \quad \mathbf{q}_T^T \quad \mathbf{q}_I^T \quad \mathbf{q}_{BL}^T \quad \mathbf{q}_{TL}^T \quad \mathbf{q}_{BR}^T \quad \mathbf{q}_{TR}^T]^T \quad (2.77)$$

Similarly, the vector of forces/moments can be defined as:

$$\mathbf{f} = [\mathbf{f}_L^T \quad \mathbf{f}_R^T \quad \mathbf{f}_B^T \quad \mathbf{f}_T^T \quad \mathbf{f}_I^T \quad \mathbf{f}_{BL}^T \quad \mathbf{f}_{TL}^T \quad \mathbf{f}_{BR}^T \quad \mathbf{f}_{TR}^T]^T \quad (2.78)$$

Application of the unit-cell analysis leads to an eigenvalue problem whose form depends again on the nature of the solution sought. The solution can then be represented in diagrams that represent the wave propagation in the frequency range of interest [Manconi 2008].

### 2.4.1 Bloch's theorem and wave propagation

In order to analyze the stop band behavior of infinite two-dimensional structures, it is required to make use of the Bloch's theorem which allows to reduce the problem through the modeling of one single unit-cell [Claeys 2013]. In solid state physics, Bloch generalized Floquet's results for two- and three-dimensional systems [Farzbod 2010]. The application to two-dimensional elastodynamical problem was then proposed leading to general forms for computing the dispersion relations [Collet 2011].

Firstly, the position vector of an arbitrary point inside the analyzed unit-cell with respect to a reference unit-cell is given by:

$$\mathbf{p} = \mathbf{p}_{ref} + n_1 \mathbf{d}_1 + n_2 \mathbf{d}_2 \quad (2.79)$$

where  $\mathbf{p}_{ref}$  is the position vector of that arbitrary point inside any unit-cell with respect to its local coordinate system. These vectors can be visualized in figure 2.7.

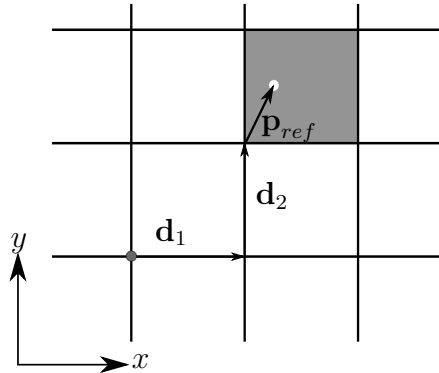


**Figure 2.7:** Schematic representation of a unit-cell in an arbitrary position within an infinite two-dimensional periodic structure

The Bloch's theorem states then that the dynamic behavior of a two-dimensional periodic system can be expressed in terms of the response of a representing unit-cell. When a time-harmonic wave travels from one unit-cell to other along two directions at frequency  $\omega$ , the relative change in wave amplitude  $V(\mathbf{p})$  that occurs is independent of the unit-cell position within the periodic structure [Claeys 2013]. This leads to the following expression:

$$V(\mathbf{p}) = V(\mathbf{p}_{ref}) e^{-i\kappa \cdot (\mathbf{d}_1 + \mathbf{d}_2)} \quad (2.80)$$

where  $V(\mathbf{p}_{ref})$  is a certain disturbance that propagates as a plane wave along planes perpendicular to the directions of propagation and  $\kappa$  represents the wave vector that expresses the amplitude decay and phase change of a wave per unit length in direction  $x$  and  $y$ . In general, the wave vectors are expressed in terms of the length through the propagation constants as follows:

$$k_x = -i\kappa_x L_x \quad (2.81)$$

and

$$k_y = -i\kappa_y L_y \quad (2.82)$$

When the propagation constants are imaginary, the waves propagate freely without attenuation. However, if the propagation constants are complex, the real part is responsible for causing exponential decay of the wave amplitude whereas the imaginary part causes the change in phase with distance. For two-dimensional structures,  $L_x$  and  $L_y$  represent the magnitude of  $\mathbf{d}_1$  and  $\mathbf{d}_2$ , which are the basis vectors of the unit-cell. On the other hand,  $n_1$  and  $n_2$  are the magnitude of  $\mathbf{n}_1$  and  $\mathbf{n}_2$ , which are vectors that express the number of unit-cells moved in  $x$  and  $y$  direction with respect to a reference unit-cell [Claeys 2013].

## 2.4.2 Boundary conditions for two-dimensional unit-cell

The analysis considers free wave motion and no external loads are taken into account. However, the forces/moment vector is different from zero since the nodal forces transmit the wave motion from one unit-cell to the next one. According to [Langley 1992], the degrees of freedom of the nodes can be related to each other in the following way:

$$\mathbf{q}_R = e^{i|k_x|} \mathbf{q}_L \quad (2.83a)$$

$$\mathbf{q}_T = e^{i|k_y|} \mathbf{q}_B \quad (2.83b)$$

$$\mathbf{q}_{BR} = e^{i|k_x|} \mathbf{q}_{BL} \quad (2.83c)$$

$$\mathbf{q}_{TL} = e^{i|k_y|} \mathbf{q}_{BL} \quad (2.83d)$$

$$\mathbf{q}_{TR} = e^{i(|k_x|+|k_y|)} \mathbf{q}_{BL} \quad (2.83e)$$

Similarly, [Langley 1992] gave the analogous conditions for the loads as follows:

$$\mathbf{f}_R = -e^{i|k_x|} \mathbf{q}_L \quad (2.84a)$$

$$\mathbf{f}_T = -e^{i|k_y|} \mathbf{q}_B \quad (2.84b)$$

$$\mathbf{f}_{BR} = -e^{i|k_x|} \mathbf{q}_{BL} \quad (2.84c)$$

$$\mathbf{f}_{TL} = -e^{i|k_y|} \mathbf{q}_{BL} \quad (2.84d)$$

$$\mathbf{f}_{TR} = e^{i(|k_x|+|k_y|)} \mathbf{q}_{BL} \quad (2.84e)$$

This led [Langley 1992] to define the force equilibrium in the following way:

$$\mathbf{f}_T + e^{i|k_y|} \mathbf{f}_B = \mathbf{0} \quad (2.85a)$$

$$\mathbf{f}_R + e^{i|k_x|} \mathbf{f}_L = \mathbf{0} \quad (2.85b)$$

$$\mathbf{f}_{TR} + e^{i|k_x|} \mathbf{f}_{TL} + e^{i|k_y|} \mathbf{f}_{RB} + e^{i(|k_x|+|k_y|)} \mathbf{f}_{BL} = \mathbf{0} \quad (2.85c)$$

### 2.4.3 Irreducible Brillouin contour and band structure

The concept of a Brillouin zone was developed by Leon Brillouin in 1930, when he worked on the propagation of electron waves in a crystal lattice. Further research transferred the concepts to elastodynamics, where a unit-cell in the wave domain is called Brillouin zone.

Due to the periodicity of the analyzed structure, the dispersion curves will be also periodic and hence not the entire wave domain have to be investigated. Furthermore, due to the possible symmetry of a unit-cell, the Brillouin zone can be reduced to an irreducible Brillouin zone which is the smallest zone in the wave space that comprehends sufficient information to obtain the band gaps [Claeys 2013].

This means that it is enough and computationally less expensive to inspect the so-called irreducible Brillouin zone to study two-dimensional wave propagation in periodic structures. If the unit-cell is limited to a symmetric rectangular unit-cell, the irreducible Brillouin zone will be only the contour with corner points  $O = (0, 0)$ ,  $A = (0, \frac{\pi}{L_y})$ ,  $B = (\frac{\pi}{L_x}, \frac{\pi}{L_y})$ ,  $O = (0, 0)$  as shown in figure 2.8 [Claeys 2013].

Typically, a two-dimensional plot called band structure is used to study the frequency ranges of stop bands, when no damping is considered in the analysis. This is obtained by varying the wave numbers  $\kappa_x$  and  $\kappa_y$  with respect to frequency along the contour of the irreducible Brillouin contour (O-A-B-O) [Zhou 2014]. The number of bands and therefore the number of waveforms, depend on the number of nodal degrees of freedom chosen for the modeling [Manconi 2008].

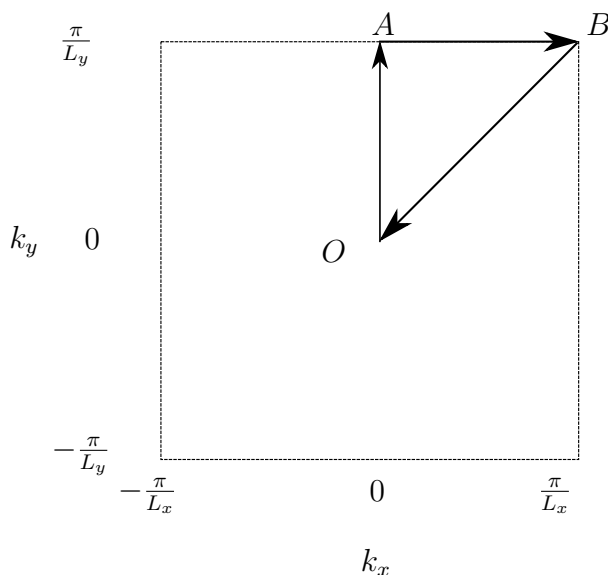


**Figure 2.8:** Irreducible Brillouin zone in a two-dimensional unit-cell

### 2.4.4 Inverse approach

In the inverse approach it is assumed free wave propagation, leading to imaginary propagation constants [Claeys 2013]. Demanding compatible displacements and force balance at the boundaries of the unit-cell, a reduction matrix  $\mathbf{R}$ , in terms of the wave propagation constants  $k_x$  and  $k_y$ , can be derived as follows:

$$\mathbf{R} = \begin{bmatrix} \mathbf{I} & \mathbf{Z} & \mathbf{Z} & \mathbf{Z} \\ \mathbf{I}e^{i|k_x|} & \mathbf{Z} & \mathbf{Z} & \mathbf{Z} \\ \mathbf{Z} & \mathbf{I} & \mathbf{Z} & \mathbf{Z} \\ \mathbf{Z} & \mathbf{I}e^{i|k_y|} & \mathbf{Z} & \mathbf{Z} \\ \mathbf{Z} & \mathbf{Z} & \mathbf{I} & \mathbf{Z} \\ \mathbf{Z} & \mathbf{Z} & \mathbf{Z} & \mathbf{I} \\ \mathbf{Z} & \mathbf{Z} & \mathbf{Z} & \mathbf{I}e^{i|k_y|} \\ \mathbf{Z} & \mathbf{Z} & \mathbf{Z} & \mathbf{I}e^{i|k_x|} \\ \mathbf{Z} & \mathbf{Z} & \mathbf{Z} & \mathbf{I}e^{i(|k_x|+|k_y|)} \end{bmatrix} \quad (2.86)$$

The reduction matrix  $\mathbf{R}$  allows to reduce the degree of freedom of the system. These reduced degree of freedom can be arranged in a vector as follows:

$$\mathbf{q}^{red} = [\mathbf{q}_L^T \ \mathbf{q}_B^T \ \mathbf{q}_I^T \ \mathbf{q}_{BL}^T]^T \quad (2.87)$$

which allows to put the vector  $\mathbf{q}$  in terms of the reduction matrix  $\mathbf{R}$  and the reduced degree of freedom vector  $\mathbf{q}^{red}$  in the following way:

$$\mathbf{q} = \begin{bmatrix} \mathbf{q}_L \\ \mathbf{q}_R \\ \mathbf{q}_B \\ \mathbf{q}_T \\ \mathbf{q}_I \\ \mathbf{q}_{BL} \\ \mathbf{q}_{TL} \\ \mathbf{q}_{BR} \\ \mathbf{q}_{TR} \end{bmatrix} = \begin{bmatrix} \mathbf{I} & \mathbf{Z} & \mathbf{Z} & \mathbf{Z} \\ \mathbf{I}e^{i|k_x|} & \mathbf{Z} & \mathbf{Z} & \mathbf{Z} \\ \mathbf{Z} & \mathbf{I} & \mathbf{Z} & \mathbf{Z} \\ \mathbf{Z} & \mathbf{I}e^{i|k_y|} & \mathbf{Z} & \mathbf{Z} \\ \mathbf{Z} & \mathbf{Z} & \mathbf{I} & \mathbf{Z} \\ \mathbf{Z} & \mathbf{Z} & \mathbf{Z} & \mathbf{I} \\ \mathbf{Z} & \mathbf{Z} & \mathbf{Z} & \mathbf{I}e^{i|k_y|} \\ \mathbf{Z} & \mathbf{Z} & \mathbf{Z} & \mathbf{I}e^{i|k_x|} \\ \mathbf{Z} & \mathbf{Z} & \mathbf{Z} & \mathbf{I}e^{i(|k_x|+|k_y|)} \end{bmatrix} \begin{bmatrix} \mathbf{q}_L \\ \mathbf{q}_B \\ \mathbf{q}_I \\ \mathbf{q}_{BL} \end{bmatrix} = \mathbf{R}\mathbf{q}^{red} \quad (2.88)$$

If the complex conjugate of the matrix  $\mathbf{R}$  is defined, the equation of motion is given by:

$$\mathbf{R}^{*T}(-\omega^2\mathbf{M} + \mathbf{K})\mathbf{R}\mathbf{q}^{red} = \mathbf{R}^{*T}\mathbf{F} \quad (2.89)$$

If the internal forces are equal to zero, the reduced force vector  $\mathbf{R}^{*T}\mathbf{F}$  vanishes. Therefore, the equation of motion reduces to the following eigenvalue problem:

$$(-\omega^2 \mathbf{M}^{red} + \mathbf{K}^{red}) \mathbf{q}^{red} = \mathbf{0} \quad (2.90)$$

where  $\mathbf{M}^{red} = \mathbf{R}^{*T}\mathbf{M}\mathbf{R}$  and  $\mathbf{K}^{red} = \mathbf{R}^{*T}\mathbf{K}\mathbf{R}$  are the reduced mass and stiffness matrices respectively. Solving the eigenvalue problem of 2.90 for  $\omega$ , the frequencies of free wave propagation are found [Claeys 2013].

## 2.5 Three-dimensional wave finite element method

The purpose of this section is to extend the WFEM approach to three-dimensional undamped structures. In figures 2.9, 2.10 and 2.11 is shown a three-dimensional unit-cell of lengths  $L_x$ ,  $L_y$  and  $L_z$  with the degrees of freedom corresponding to the corners, edges and faces.

The degrees of freedom can be arranged in a vector as follows:

$$\mathbf{q} = [\mathbf{q}_K^T \quad \mathbf{q}_E^T \quad \mathbf{q}_F^T]^T \quad (2.91)$$

where

$$\mathbf{q}_K = [\mathbf{q}_{K1}^T \quad \mathbf{q}_{K2}^T \quad \mathbf{q}_{K3}^T \quad \mathbf{q}_{K4}^T \quad \mathbf{q}_{K5}^T \quad \mathbf{q}_{K6}^T \quad \mathbf{q}_{K7}^T \quad \mathbf{q}_{K8}^T]^T \quad (2.92)$$

$$\mathbf{q}_E = [\mathbf{q}_{E1}^T \quad \mathbf{q}_{E2}^T \quad \mathbf{q}_{E3}^T \quad \mathbf{q}_{E4}^T \quad \mathbf{q}_{E5}^T \quad \mathbf{q}_{E6}^T \quad \mathbf{q}_{E7}^T \quad \mathbf{q}_{E8}^T \quad \mathbf{q}_{E9}^T \quad \mathbf{q}_{E10}^T \quad \mathbf{q}_{E11}^T \quad \mathbf{q}_{E12}^T]^T \quad (2.93)$$

$$\mathbf{q}_F = [\mathbf{q}_{F1}^T \quad \mathbf{q}_{F2}^T \quad \mathbf{q}_{F3}^T \quad \mathbf{q}_{F4}^T \quad \mathbf{q}_{F5}^T \quad \mathbf{q}_{F6}^T]^T \quad (2.94)$$

Similarly, the vector of forces/momenta can be defined as:

$$\mathbf{f} = [\mathbf{f}_K^T \quad \mathbf{f}_E^T \quad \mathbf{f}_F^T]^T \quad (2.95)$$

where

$$\mathbf{f}_K = [\mathbf{f}_{K1}^T \quad \mathbf{f}_{K2}^T \quad \mathbf{f}_{K3}^T \quad \mathbf{f}_{K4}^T \quad \mathbf{f}_{K5}^T \quad \mathbf{f}_{K6}^T \quad \mathbf{f}_{K7}^T \quad \mathbf{f}_{K8}^T]^T \quad (2.96)$$

$$\mathbf{f}_E = \left[ \mathbf{f}_{E1}^T \quad \mathbf{f}_{E2}^T \quad \mathbf{f}_{E3}^T \quad \mathbf{f}_{E4}^T \quad \mathbf{f}_{E5}^T \quad \mathbf{f}_{E6}^T \quad \mathbf{f}_{E7}^T \quad \mathbf{f}_{E8}^T \quad \mathbf{f}_{E9}^T \quad \mathbf{f}_{E10}^T \quad \mathbf{f}_{E11}^T \quad \mathbf{f}_{E12}^T \right]^T \quad (2.97)$$

$$\mathbf{f}_F = \left[ \mathbf{f}_{F1}^T \quad \mathbf{f}_{F2}^T \quad \mathbf{f}_{F3}^T \quad \mathbf{f}_{F4}^T \quad \mathbf{f}_{F5}^T \quad \mathbf{f}_{F6}^T \quad \right]^T \quad (2.98)$$

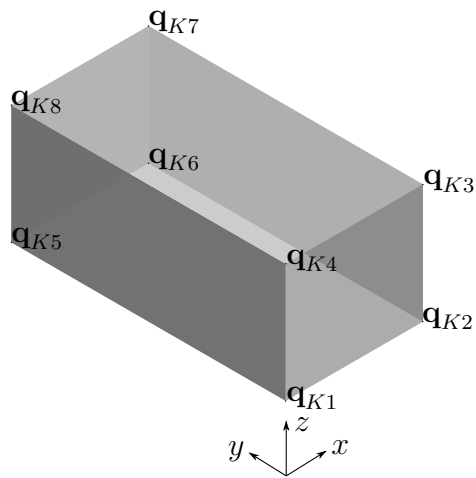


**Figure 2.9:** Three-dimensional unit-cell with its respective degrees of freedom at the corners

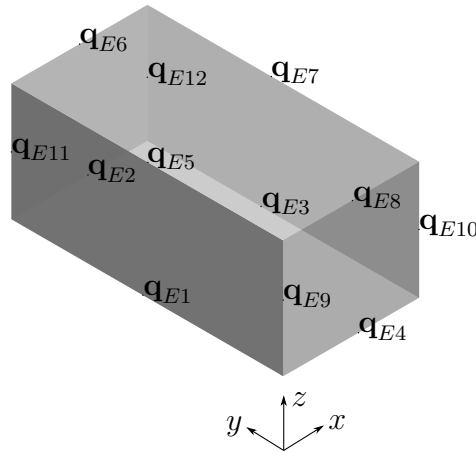


**Figure 2.10:** Three-dimensional unit-cell with its respective degrees of freedom at the edges

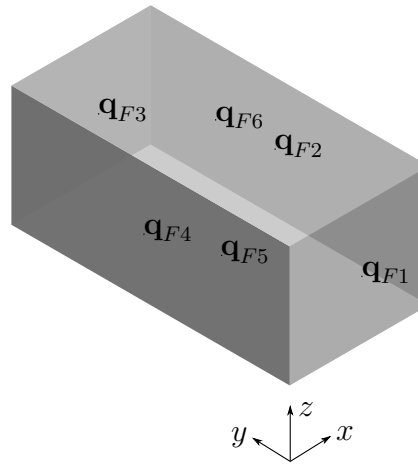


**Figure 2.11:** Three-dimensional unit-cell with its respective degrees of freedom at the faces

### 2.5.1 Inverse approach

The inverse approach is used to obtain band structures, which means that the analysis is limited to unit-cell models without damping. The unit-cell model has to be meshed with an equal number of nodes at its respective master and slave boundaries as well as it has to be meshed with an aspect ratio small compared with the wavelength of the problem. Typically, this is with ten elements per wavelength in the direction of propagation [Manconi 2008].

If these wave propagation constants are proposed, the problem aims to find the propagating frequencies or in other words solving the following eigenvalue problem for  $\omega^2$ :

$$(-\omega^2 \mathbf{M}^{red} + \mathbf{K}^{red}) \mathbf{q}^{red} = \mathbf{0} \quad (2.99)$$

where  $\mathbf{q}^{red}$  indicates the reduced general displacements/rotations vector defined by

$$\mathbf{q}^{red} = [\mathbf{q}_{K1}^T \quad \mathbf{q}_{E1}^T \quad \mathbf{q}_{E4}^T \quad \mathbf{q}_{E9}^T \quad \mathbf{q}_{F1}^T \quad \mathbf{q}_{F4}^T \quad \mathbf{q}_{F5}^T \quad \mathbf{q}_I^T]^T \quad (2.100)$$

and the positive definite Hermitian matrices

$$\mathbf{M}^{red} = \mathbf{R}^{*T} \mathbf{M} \mathbf{R} \quad (2.101a)$$

$$\mathbf{K}^{red} = \mathbf{R}^{*T} \mathbf{K} \mathbf{R} \quad (2.101b)$$

are the reduced mass and stiffness matrices respectively. For any given values of the propagation constants there will be then  $n$  real positive eigenvalues for which wave propagation is

possible, where  $n$  corresponds to the dimension of  $\mathbf{q}^{red}$  [Manconi 2008].

The reduction matrix  $\mathbf{R}$  for three-dimensional propagation is given by:

$$\mathbf{R} = \begin{bmatrix} \mathbf{I} & \mathbf{Z} \\ \mathbf{I}e^{i|k_x|} & \mathbf{Z} \\ \mathbf{I}e^{i(|k_x|+|k_z|)} & \mathbf{Z} \\ \mathbf{I}e^{i|k_z|} & \mathbf{Z} \\ \mathbf{I}e^{i|k_y|} & \mathbf{Z} \\ \mathbf{I}e^{i(|k_x|+|k_y|)} & \mathbf{Z} \\ \mathbf{I}e^{i(|k_x|+|k_y|+|k_z|)} & \mathbf{Z} \\ \mathbf{I}e^{i(|k_y|+|k_z|)} & \mathbf{Z} \\ \mathbf{Z} & \mathbf{I} & \mathbf{Z} & \mathbf{Z} & \mathbf{Z} & \mathbf{Z} & \mathbf{Z} & \mathbf{Z} \\ \mathbf{Z} & \mathbf{Z} & \mathbf{I}e^{i|k_y|} & \mathbf{Z} & \mathbf{Z} & \mathbf{Z} & \mathbf{Z} & \mathbf{Z} \\ \mathbf{Z} & & \mathbf{I}e^{i|k_x|} & \mathbf{Z} & \mathbf{Z} & \mathbf{Z} & \mathbf{Z} & \mathbf{Z} \\ \mathbf{Z} & & \mathbf{Z} & \mathbf{I} & \mathbf{Z} & \mathbf{Z} & \mathbf{Z} & \mathbf{Z} \\ \mathbf{Z} & & \mathbf{I}e^{i|k_z|} & \mathbf{Z} & \mathbf{Z} & \mathbf{Z} & \mathbf{Z} & \mathbf{Z} \\ \mathbf{Z} & & \mathbf{Z} & & \mathbf{I}e^{i(|k_y|+|k_z|)} & \mathbf{Z} & \mathbf{Z} & \mathbf{Z} \\ \mathbf{Z} & & \mathbf{I}e^{i(|k_x|+|k_z|)} & \mathbf{Z} & \mathbf{Z} & \mathbf{Z} & \mathbf{Z} & \mathbf{Z} \\ \mathbf{Z} & & \mathbf{Z} & & \mathbf{I}e^{i|k_z|} & \mathbf{Z} & \mathbf{Z} & \mathbf{Z} \\ \mathbf{Z} & & \mathbf{Z} & & \mathbf{Z} & \mathbf{I} & \mathbf{Z} & \mathbf{Z} \\ \mathbf{Z} & & \mathbf{Z} & & \mathbf{Z} & & \mathbf{I}e^{i|k_x|} & \mathbf{Z} \\ \mathbf{Z} & & \mathbf{Z} & & \mathbf{Z} & & \mathbf{I}e^{i|k_y|} & \mathbf{Z} \\ \mathbf{Z} & & \mathbf{Z} & & \mathbf{Z} & & \mathbf{I}e^{i(|k_x|+|k_y|)} & \mathbf{Z} \\ \mathbf{Z} & & \mathbf{Z} & & \mathbf{Z} & & \mathbf{Z} & \mathbf{I} \\ \mathbf{Z} & & \mathbf{Z} & & \mathbf{Z} & & \mathbf{Z} & \mathbf{I}e^{i|k_x|} \\ \mathbf{Z} & & \mathbf{Z} & & \mathbf{Z} & & \mathbf{I}e^{i|k_y|} & \mathbf{Z} \\ \mathbf{Z} & & \mathbf{Z} & & \mathbf{Z} & & \mathbf{Z} & \mathbf{I} \\ \mathbf{Z} & & \mathbf{Z} & & \mathbf{Z} & & \mathbf{Z} & \mathbf{I}e^{i|k_z|} \\ \mathbf{Z} & & \mathbf{Z} & & \mathbf{Z} & & \mathbf{Z} & \mathbf{Z} \end{bmatrix} \quad (2.102)$$

# 3 Implementation and validation

## 3.1 Implementation

In this thesis a computational tool called METAMAT (METAMaterials Tool) has been implemented for obtaining the dispersion curves and band structures in a Graphical User Interface (GUI). This tool has been designed in MATLAB® to read a finite element model from ANSYS®. During this process, the nodal and element information is obtained as well as the mass, stiffness, and damping matrices. Having read the information about the model, the tool applies one of the methods presented in the previous section to analyze a unit-cell model depending on the type of solution to be sought. For the scope of this thesis, only the dispersion curves and band structures can be obtained and presented for the user to interpret.

The first step to apply the wave finite element method is to construct a finite element model in ANSYS® of the unit-cell with certain criteria. First, a minimum number of nodes per wavelength is required to obtain an accurate solution. The conventional number of nodes should be between six and ten nodes per wavelength [Silva 2015]. Furthermore, the element technology, element aspect ratio, and physical interfaces between different materials are other important criteria to care about. Finally, the consistency in the ordering of slave boundary nodes with respect to the master boundary nodes as shown in figure 3.1 is an important constraint to mesh the model of the unit-cell [Mace 2005].

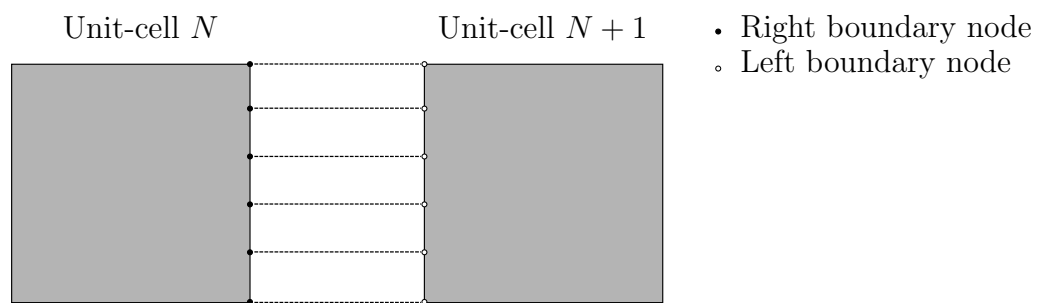


**Figure 3.1:** Coupling of nodes between two unit-cells

After having obtained a model which fulfills the discussed criteria, the second step is to obtain the mass, stiffness, and proportional damping matrices from ANSYS®. This process is shown in figure 3.2, which was based on the technical note of [Batailly 2012]. The extraction has to be without the consideration of any boundary condition. However, if the model has TMDs, the restrictions have to be reflected in the matrices.

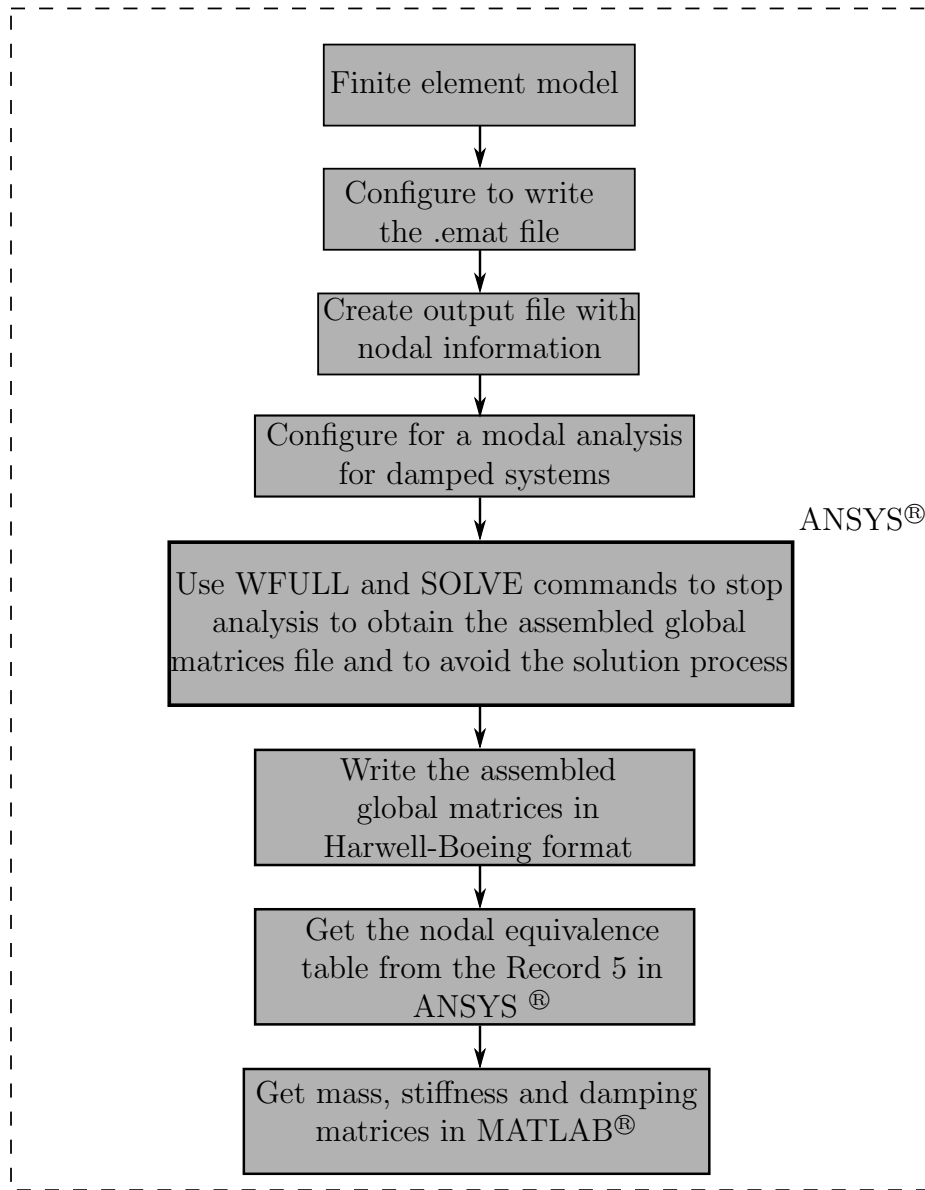


**Figure 3.2:** Flowchart of the code implementation for the extraction of  $\mathbf{M}$ ,  $\mathbf{C}$  and  $\mathbf{K}$  from ANSYS®

As a remark, the mass, stiffness, and damping matrices are obtained from ANSYS® as assembled global matrices in Harwell-Boeing format. This format is used to efficiently store a sparse matrix in a column-oriented matter. In addition to that, the ANSYS® commands

WRFULL and SOLVE have to be used to make the analysis stop before doing the analysis so that the matrices will remain consistent. Once the matrices are in this format, the retrieval of the information is performed using a MATLAB® program retrieved from [Burkardt 2017].

As a third point, the file of the ANSYS® model in format .inp or .txt and the specification of the analysis that have to be performed must be specified in the GUI. The band structure or the dispersion relations are available at the end of the computation. The flowchart of this last step is shown in figure 3.3.

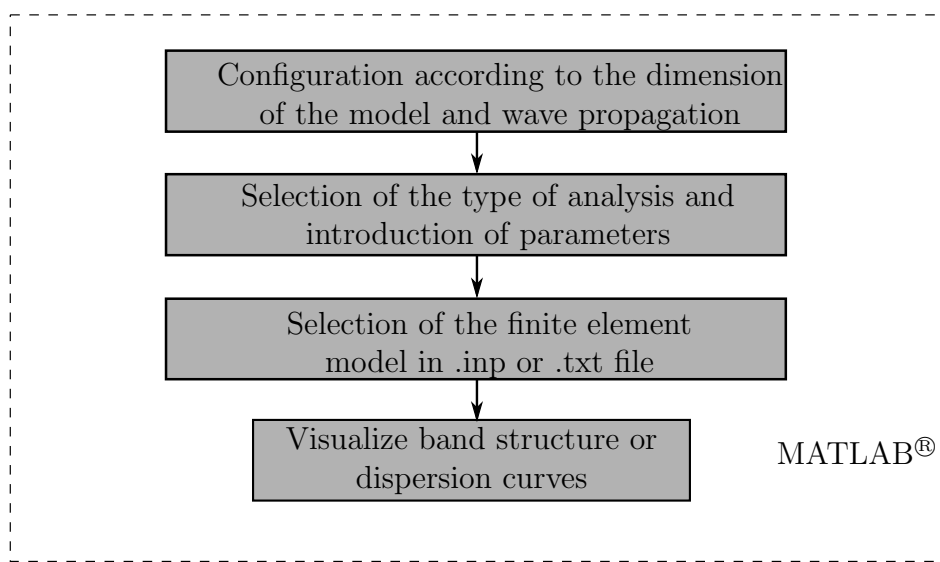


**Figure 3.3:** Flowchart of the code implementation for the tool METAMAT

As a final remark, it is recommended to work with the ANSYS® elements of the following table:

Wave propagation	Dimension of the model	Element type
1D	1D	BEAM3
1D	2D	PLANE182 with enhanced strain formulation
1D	3D	SOLID185 with enhanced strain formulation
2D	2D	SHELL63
3D	3D	SOLID185 with enhanced strain formulation

**Table 3.1:** Recommended element types in ANSYS® for modeling a unit-cell

This section described the developed computational tool to obtain the dispersion diagrams and band structures. The details of the code files and the implementation are presented in the appendix.

## 3.2 Benchmark problem for one-dimensional unit-cell

This section presents three benchmark examples that are used to assess the performance of the developed tool METAMAT. The results of these experiments are performed and validated according to the work of [Claeys 2013].

### 3.2.1 Infinite Euler-Bernoulli beam

The first benchmark problem is an infinite Euler-Bernoulli undamped beam. This example is computationally non-expensive and provides a very good grasp to the wave propagation in one dimension. The table 3.2 summarizes the characteristics of the unit-cell.

Property	Symbol	Value
Young's modulus	$E$	210 GPa
Poisson's ratio	$\nu$	0.3
Density	$\rho$	7800 kg/m <sup>3</sup>
Cross-sectional area	$A$	10 <sup>-4</sup> m <sup>2</sup>
Second moment of inertia	$I$	8.33 × 10 <sup>-10</sup> m <sup>4</sup>
Length	$L_x$	1 m
Weight	$W$	0.78 kg

**Table 3.2:** Material characteristics and dimensions of a one-dimensional unit-cell

This experiment aims to analyze a one-, two-, and three-dimensional unit-cell under one-dimensional propagation. Figure 3.4 shows the dispersion curves of the models, using the propagation constant  $k = -i\kappa L_x$  and the frequency  $f$ . As a remark, the propagation constant itself can be considered dimensionless according to [Claeys 2013].

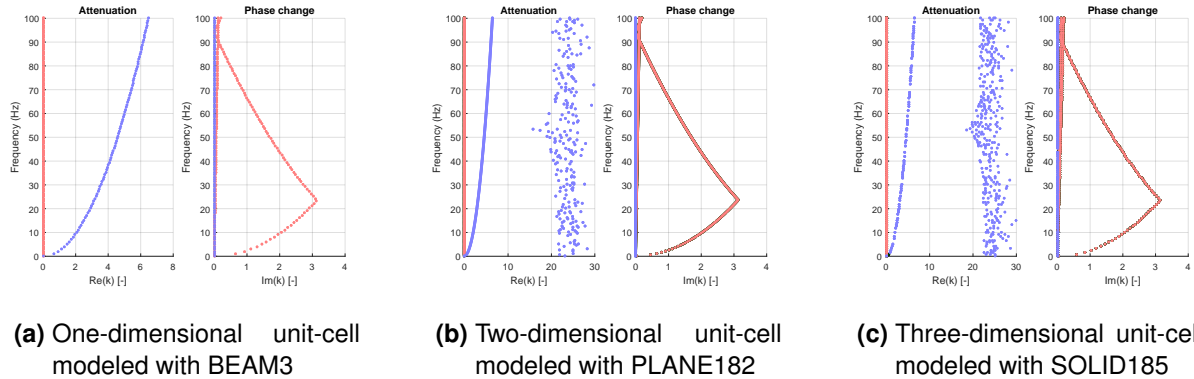


**Figure 3.4:** Dispersion curves of the freely propagating waves in positive direction from 0 to 100 Hz of an infinite Euler-Bernoulli beam modeled with different type of elements

The blue and red colors represent the evanescence and the free propagating waves respectively, in both negative and positive direction. As these models do not consider damping, the real part stays in zero for non-zero phase. However, if the phase is zero, the respective real part may represent the rigid body modes.

According to [Claeys 2013], the frequency of the stop band depends on the length of the unit-cell and the wavelength. When the phase shift reaches  $\pi$  for the first time, the wavelength equals twice the unit-cell length, so that destructive interference is possible [Mace 2005]. For this case,  $\pi$  is reached at 23.52 Hz for bending waves. A theoretical way to validate this is using the following formula:

$$f = \frac{\pi}{2L_x^2} \sqrt{\frac{EI}{\rho A}} \quad (3.1)$$

Introducing the values of the table 3.2 in equation 3.1 for an infinite Euler-Bernoulli beam gives a frequency of 23.52 Hz which coincides with the result given by the dispersion curves [Claeys 2013]. The inverse approach can also be used since there is no damping in the model. Figure 3.5 gives the band structure of the same unit-cell, showing that a phase shift equal to  $\pi$  is reached at 23.52 Hz.

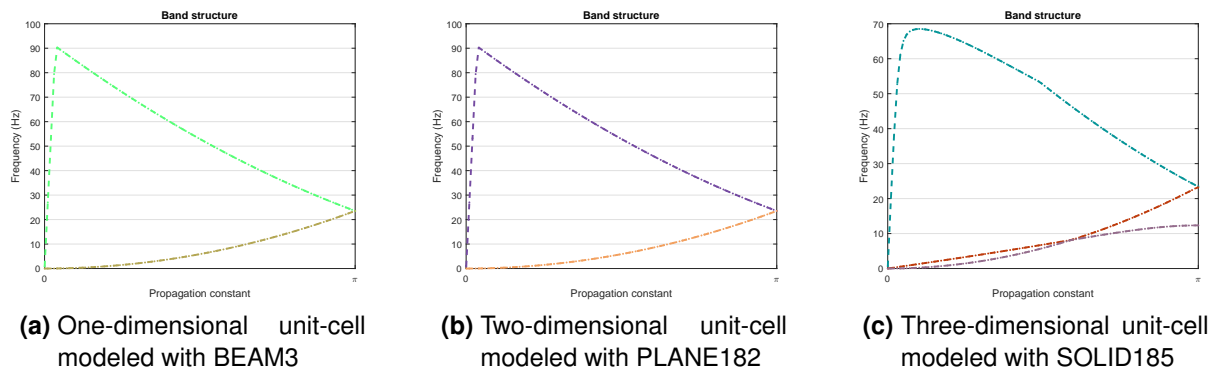


**Figure 3.5:** Band structure of the first two bands of an infinite Euler-Bernoulli beam

As it was mentioned in the theoretical section, there are mainly three ways to obtain the dispersion curves through the direct approach. These are the traditional WFEM, the CWFEM, and the method developed by Zhong or ZWFEM. Figures 3.6, 3.7 and 3.8 show the plots obtained by using these three solvers on the three models.

In figures 3.9, 3.10 and 3.11 the range of analysis is from 0 to 5000 Hz, which shows the consistency in results for the three solvers. It is also seen that other types of waves, besides

the bending waves, appear. This is because the speed of longitudinal waves and shear waves is dominated by different properties as it was mentioned in section 2.1.4.

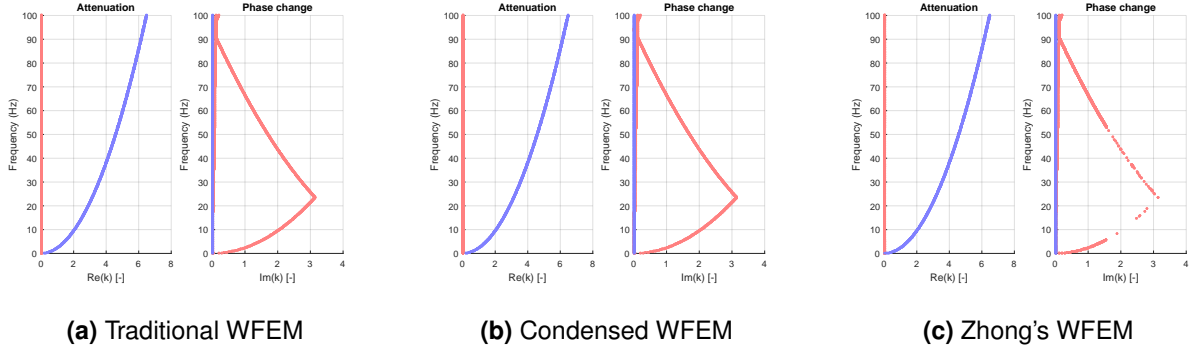


**Figure 3.6:** Dispersion curves of the freely propagating waves in positive direction from 0 Hz to 100 Hz of a one-dimensional model using different solvers

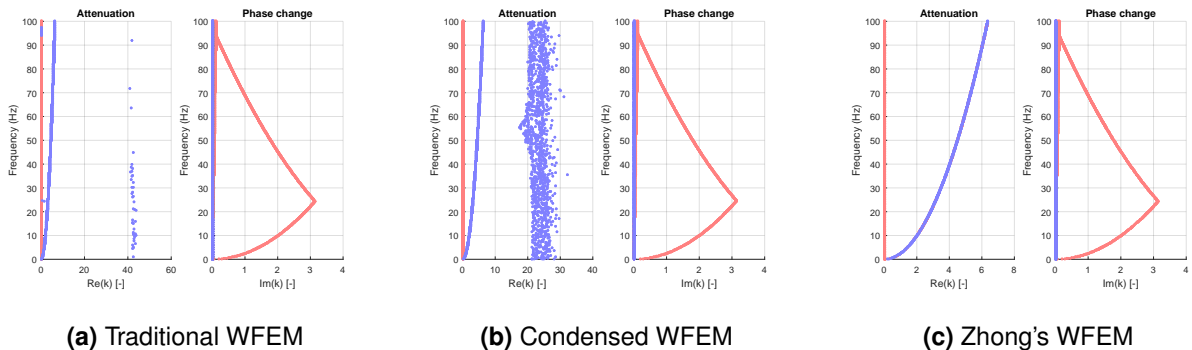


**Figure 3.7:** Dispersion curves of the freely propagating waves in positive direction from 0 Hz to 100 Hz of a two-dimensional model using different solvers

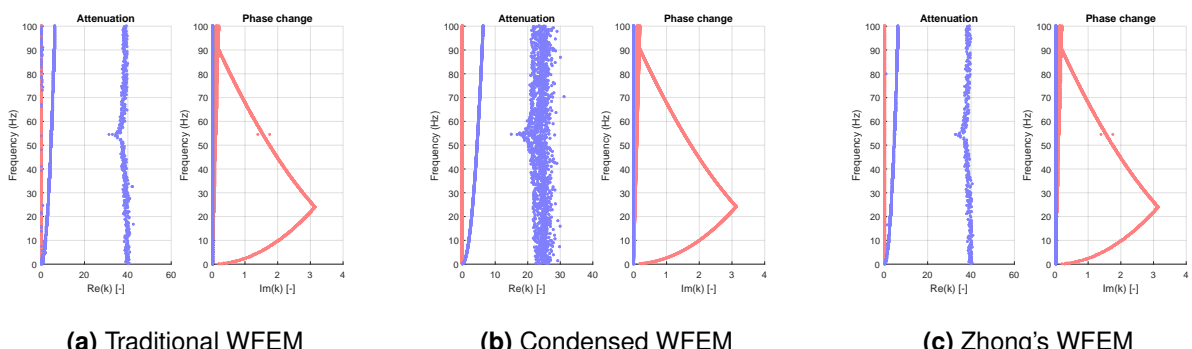


**Figure 3.8:** Dispersion curves of the freely propagating waves in positive direction from 0 Hz to 100 Hz of a three-dimensional model using different solvers

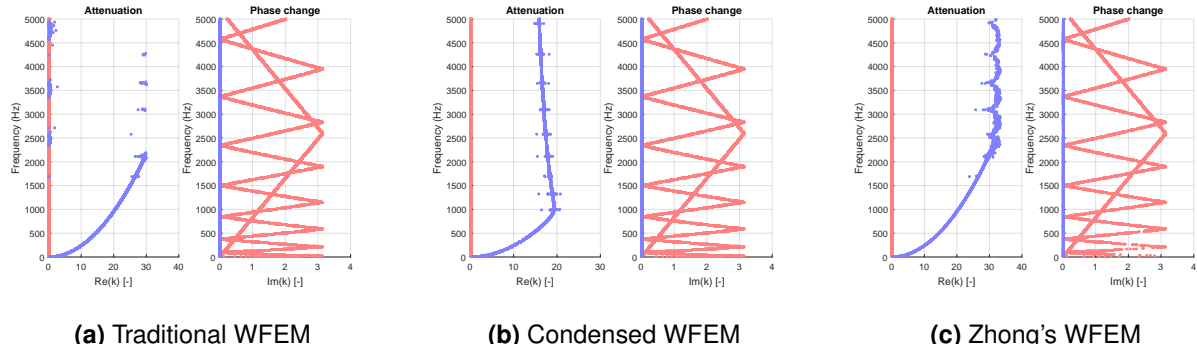


**Figure 3.9:** Dispersion curves of the freely propagating waves in positive direction from 0 to 5000 Hz of a one-dimensional model using different solvers

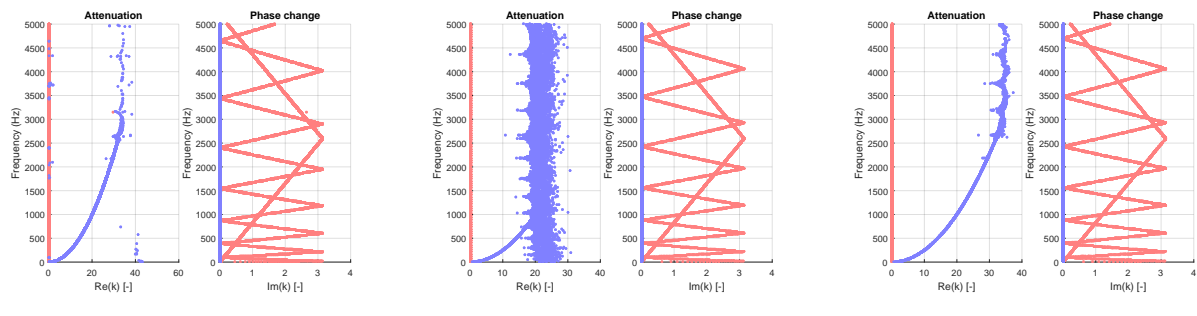


**Figure 3.10:** Dispersion curves of the freely propagating waves in positive direction from 0 to 5000 Hz of a two-dimensional model using different solvers

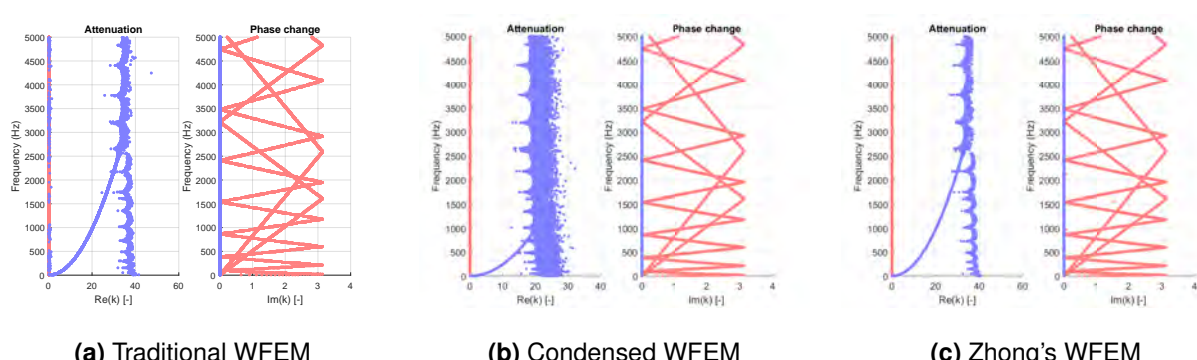


**Figure 3.11:** Dispersion curves of the freely propagating waves in positive direction from 0 to 5000 Hz of a three-dimensional model using different solvers

### 3.2.2 Infinite Euler-Bernoulli beam with a punctual mass

This section aims to present the behavior of the original test case but taking into consideration the effect of adding a punctual mass to the beam. The test is made with one punctual mass without rotational inertia located at the end of each unit-cell. Figure 3.12 show that the wave propagates freely in positive direction until it reaches a phase shift of  $\pi$ , which provokes a jump between 19.8 Hz and 23.6 Hz. This is due to the fact that the waves are partially reflected at the punctual mass in this interval of frequency, so that no free propagation is possible and the stop bands can be detected. For higher frequencies the waves behave again like free propagating waves [Claeys 2013].

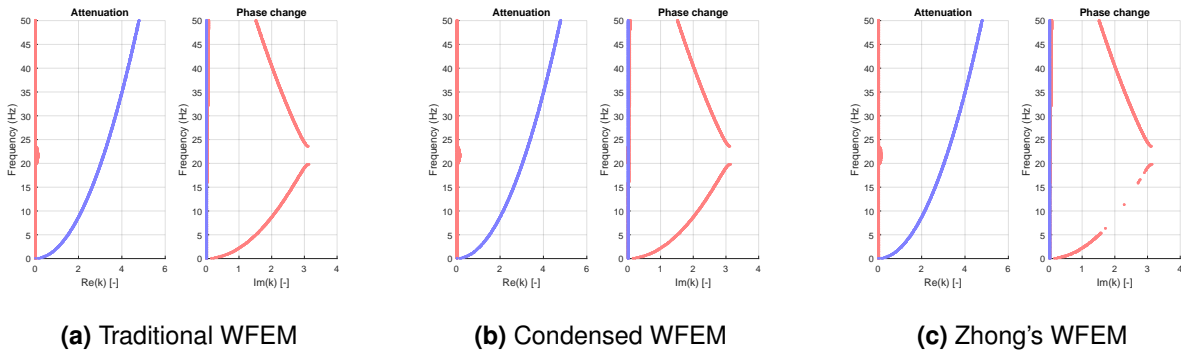


**Figure 3.12:** Dispersion curves of the freely propagating waves in positive direction from 0 to 50 Hz of a one-dimensional model with an added mass of 0.156 kg using different solvers

In order to see the effect of the additional mass, figure 3.12 shows the effect of different values of masses. For increasing mass, the jump where the stop band takes place is bigger.

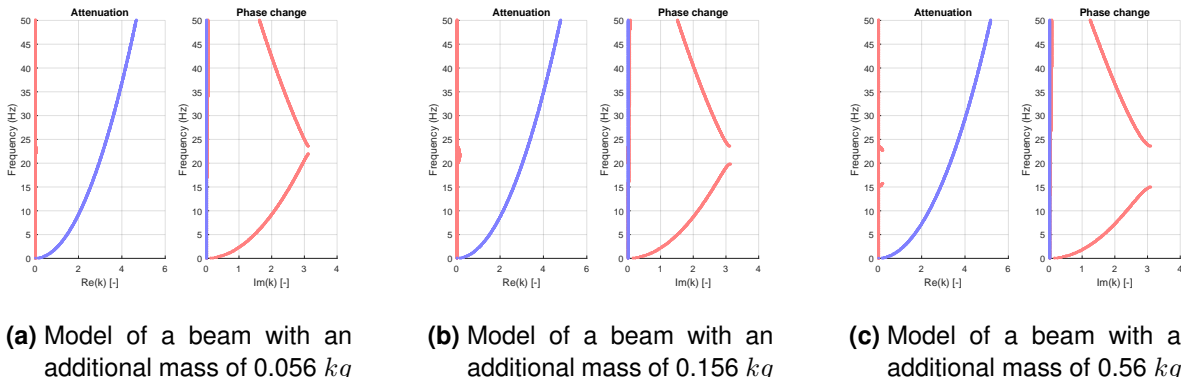


**Figure 3.13:** Dispersion curves of the freely propagating waves in positive direction from 0 to 50 Hz of a one-dimensional model with a punctual mass. The mass has different values to see the effect of increasing mass

### 3.2.3 Infinite Euler-Bernoulli beam with a spring-mass system

This section aims to present the dynamic behavior of the original test case but taking into consideration the effect of adding a resonator to the beam. The test is made with a spring-mass system located at the end of each unit-cell according to [Claeys 2013]. This additional single degree of freedom system can also lead to a stop band, depending on the values chosen for the spring and mass as shown in figure 3.14.

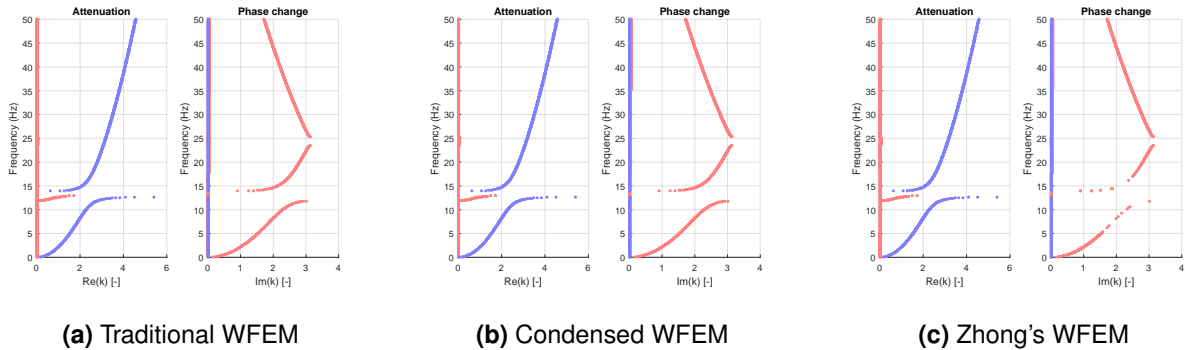


**Figure 3.14:** Dispersion curves of the freely propagating waves in positive direction from 0 to 50 Hz of a one-dimensional model with an spring-mass system using different solvers. The spring-mass system consists of a mass of 0.156 kg and a spring of 1000 N/m

If the resonance frequency of the spring-mass system is reached, the wave has complex propagation constants and a band gap appears. After that, a interference band gap can be found. Figure 3.15 shows how the resonance stop band can be manipulated with different values of stiffness.

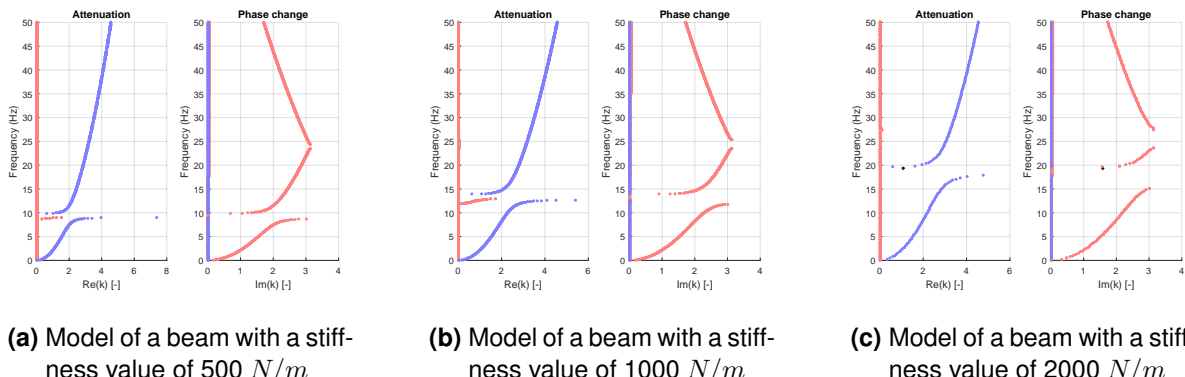


**Figure 3.15:** Dispersion curves from 0 to 50 Hz of one-dimensional model with a spring-mass system. The curves show that the resonance frequency of the resonator appears before the stop band and the increasing of the bandwidth for vibration reduction as the stiffness raises

### 3.2.4 Infinite Euler-Bernoulli beam with a TMD

This section aims to study the dynamic behavior of the original test case but taking into consideration the effect of adding a TMD to the beam. The test is made with a TMD located at the end of each unit-cell according to [Claeys 2013]. When damping is introduced, the stop band gets more difficult to be identified in the dispersion curves. Figure 3.16 shows the dispersion curves of this system using the available solvers.

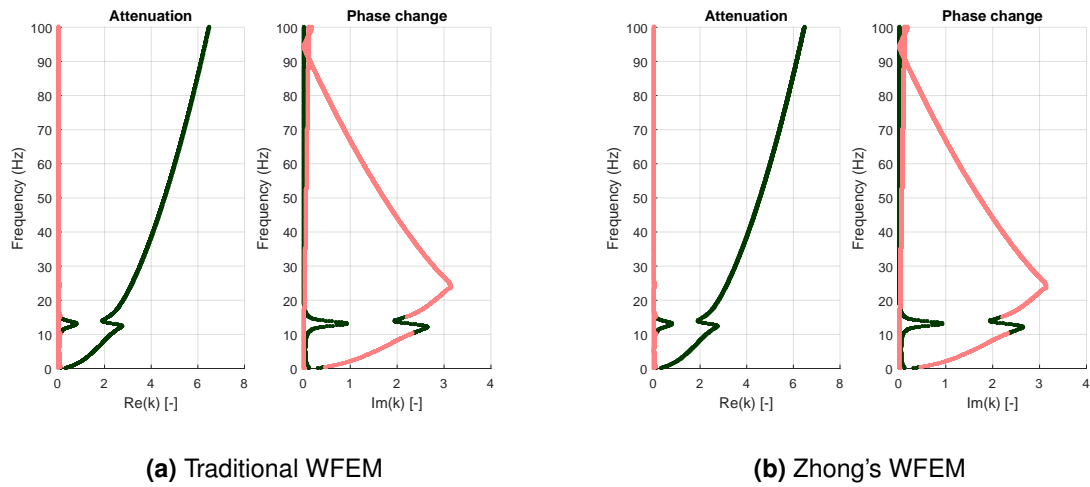


**Figure 3.16:** Dispersion curves from 0 to 100 Hz of one-dimensional model with a TMD

In order to see the effect of the damping, figure 3.17 shows the effect of different values of damping ratios for the TMD. The addition of a TMD broadens the zone of influence, but decreases the response of the TMD [Claeys 2013].

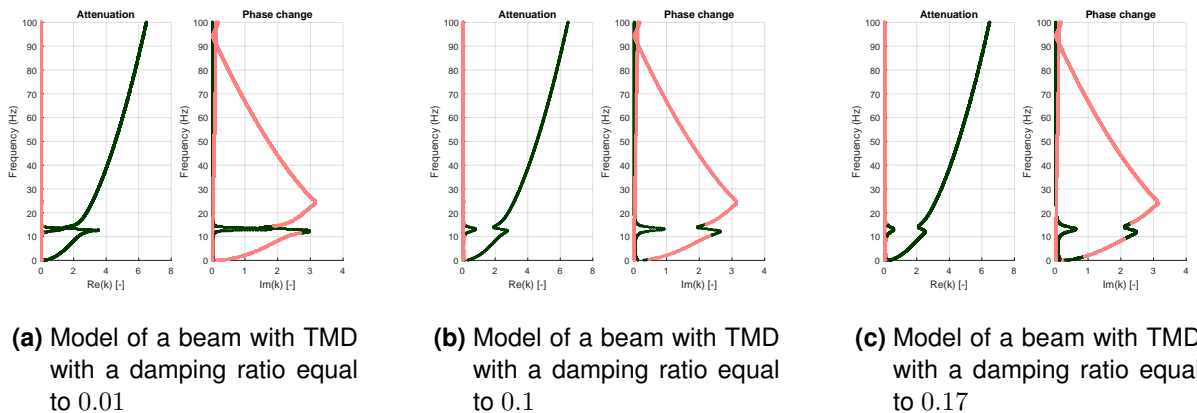


**Figure 3.17:** Dispersion curves from 0 to 100 Hz of one-dimensional model with a TMD. The plots show the influence of three different values of damping ratios for the attached TMD

### 3.2.5 Comparison of methods

This section presents the comparison between different solvers and methods for one-dimensional wave propagation. Figure 3.18 shows the plot of the computational time of the analysis with different solvers vs the number of steps. The number of steps are the number of times that the eigenvalue problem has to be solved for a specific method. The more steps the better the resolution of the dispersion curves.

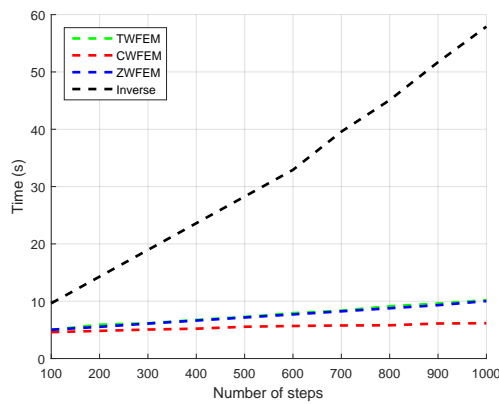


**Figure 3.18:** Computational time of the analysis of a one-dimensional model with 300 degrees of freedom using different solvers vs the number of steps

This analysis suggests that the CWFEM is the fastest method from the four ways to perform the analysis. The plot also shows the linear behavior of the analysis when the number of steps increases, whereas Figure 3.19 shows the non-linear behavior of the analysis as the number of degrees of freedom increases. This experiment was performed with 300 steps.

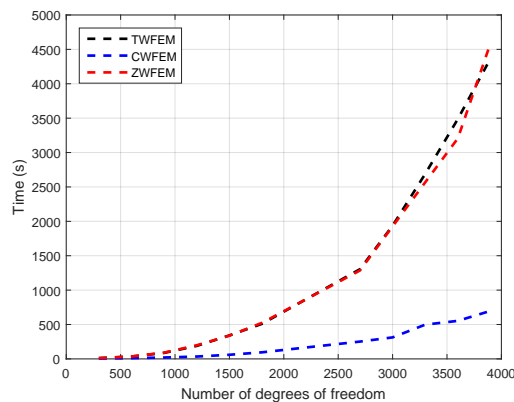


**Figure 3.19:** Computation time of the analysis of a one-dimensional model with different solvers vs the number of degrees of freedom

### 3.3 Benchmark problem for two-dimensional unit-cell

#### 3.3.1 Plate

This section aims to study the vibrational behavior of a two-dimensional undamped unit-cell in an infinite structure through the inverse approach [Claeys 2013]. The table 3.3 summarizes the characteristics of the unit-cell.

Property	Symbol	Value
Young's modulus	$E$	210 GPa
Poisson's ratio	$\nu$	0.3
Density	$\rho$	7800 kg/m <sup>3</sup>
Thickness	$t$	1 mm
Length in x direction	$L_x$	1 m
Length in y direction	$L_y$	1 m

**Table 3.3:** Material characteristics and dimensions of a two-dimensional unit-cell

The first experiment studies the vibrational behavior of the plate without periodic elements such as punctual masses or spring-mass systems. Due to the symmetry of the unit-cell, the analysis can be reduced to the analysis of the irreducible Brillouin zone with corner points  $O = (0, 0)$ ,  $A = (0, \pi)$ ,  $B = (\pi, \pi)$ ,  $O = (0, 0)$  [Claeys 2013]. Figure 3.20 shows the band structure of this unit-cell along the irreducible Brillouin contour.

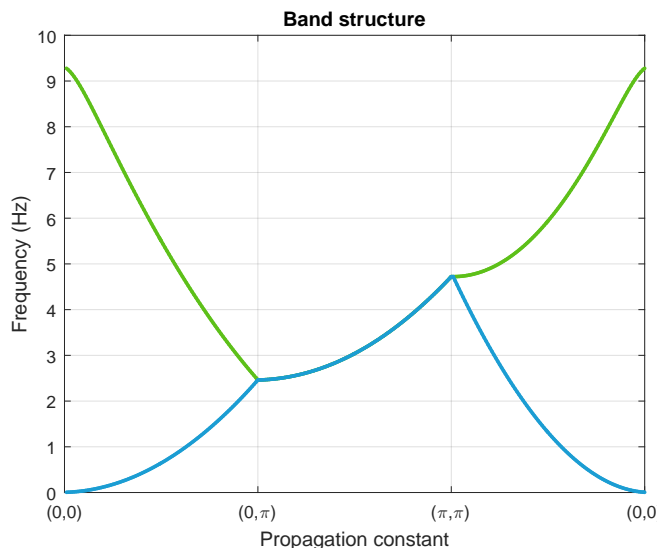


**Figure 3.20:** Band structure of a plate. The two first bands are shown along the irreducible Brillouin contour.

Figure 3.21 shows the band structures of a plate without any elements, a plate with a punctual mass located in the center, and a plate with a spring-mass system located in the center. The aim is to visualize the effect of each element on the unit-cell.

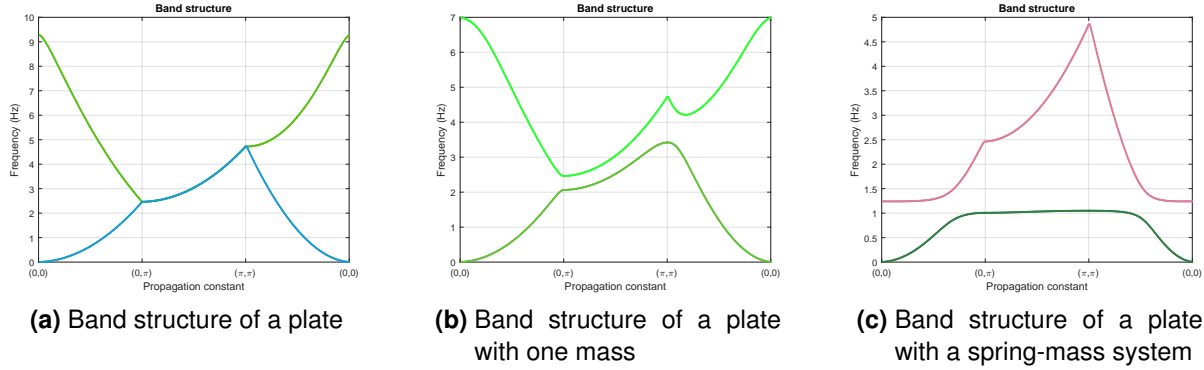


**Figure 3.21:** Band structure of a plate with different configurations

For the case of the plate without any resonator, the frequency for which the wavelength equals twice the unit-cell length can be computed, according to [Claeys 2013], by:

$$f = \frac{\pi}{2L_x^2} \sqrt{\frac{Et^2}{12(1 - \nu^2)\rho}} \quad (3.2)$$

Introducing the values of table 3.3 in equation 3.2, a value of 2.46 Hz is obtained which coincides with the value from the band structure in the range from  $O = (0, 0)$  to  $A = (0, \pi)$  in figure 3.21a. It can also been seen that there are not band gaps associated to this model, but they appear as soon as a mass or a spring-mass system is added as shown in figures 3.21b and 3.21c. They can also be manipulated as shown in figures 3.22 and 3.23. The full interpretation can be found in [Claeys 2013].

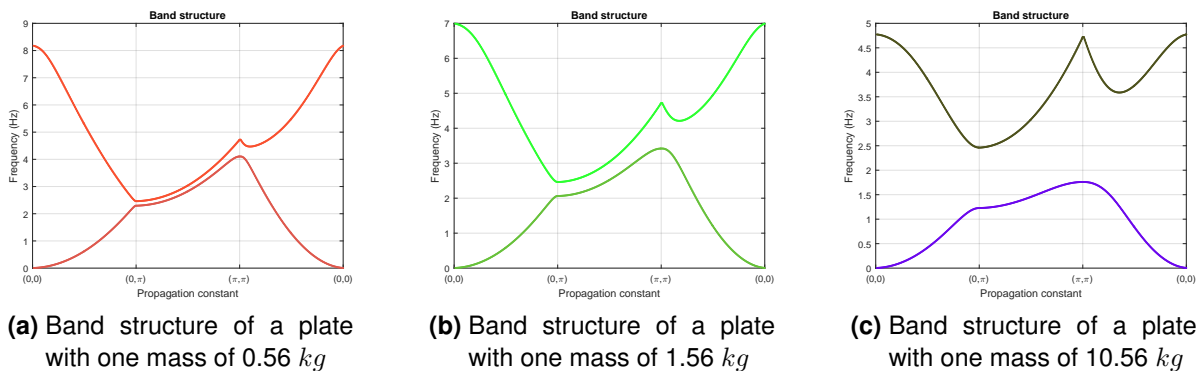


**Figure 3.22:** Band structure of a plate with a punctual mass in the center. The value of the mass is variable

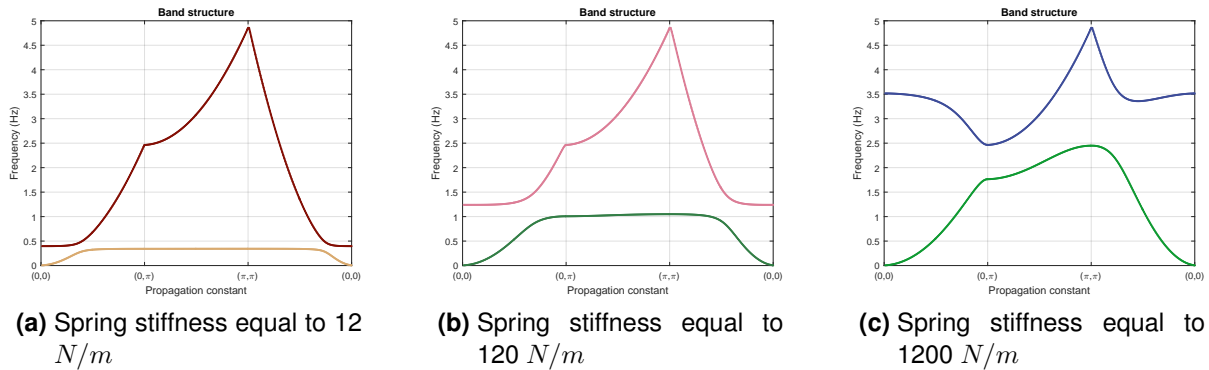


**Figure 3.23:** Band structure of a plate with a spring-mass system. The value of the spring stiffness is variable

### 3.4 Benchmark problem for three-dimensional unit-cell

This section aims to study the vibrational behavior of a three-dimensional unit-cell, using an infinite undamped cube as a test case through the inverse approach. The table 3.4 summarizes the characteristics of the unit-cell.

Property	Symbol	Value
Young's modulus	$E$	210 GPa
Poisson's ratio	$\nu$	0.3
Density	$\rho$	7800 kg/m <sup>3</sup>
Length in x direction	$L_x$	1 m
Length in y direction	$L_y$	1 m
Length in z direction	$L_z$	1 m

**Table 3.4:** Material characteristics and dimensions of a three-dimensional unit-cell

The experiment studies the vibrational behavior of the unit-cell which can be further reduced by analyzing the irreducible Brillouin zone with corner points  $O = (0,0,0)$ ,  $A = (0,\pi,0)$ ,  $B = (0,\pi,\pi)$ ,  $C = (\pi,\pi,\pi)$ ,  $O = (0,0,0)$  [Claeys 2013]. Figure 3.24 shows the band structure of this unit-cell along the irreducible Brillouin contour.

Up to now, there is no theoretical formulation to validate the obtained results. However, the formulation of the three-dimensional inverse method fulfills the theory of the wave finite element method given by [Claeys 2013].

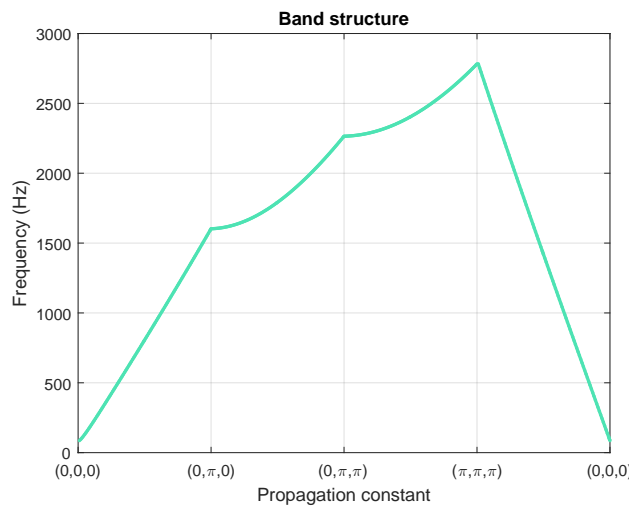


**Figure 3.24:** Band structure of a three-dimensional unit-cell. The first band is shown along the irreducible Brillouini contour

## 3.5 Numerical errors

This section aims to present the numerical errors that arise due to WFEM. In general there are three types of errors, discretization errors, round-off errors and truncation errors. In order to obtain the maximum accuracy level of the method, it is important to detect the sources that bring these errors [Silva 2015].

First of all, if the finite element model do not follow the criteria of modeling such as the number of elements or the correct aspect ratio, the results will be inaccurate. It was mentioned that there is a minimum number of elements per wavelength that is required for the WFEM to obtain accurate solutions. The recommendation is that the element size should be at least one tenth of the wavelength in the structure, otherwise the model will become inaccurate. According to [Silva 2015], when multiple wave modes are involved, the minimum element size is related to the wave mode in the dispersion diagram. This means that the higher is the frequency, the higher the number of elements needed. The size of the element can be determined by:

$$\frac{L_x}{4n} > e \quad (3.3)$$

where  $e$  is the element size and  $n$  the number of crosses by  $\pi$  or zero in the dispersion diagram. However, if the size of the element is very small in comparison to the shortest wavelength of

interest, machine round-errors arise [Mace 2005]. For example, figure 3.25 shows a dispersion diagram with extremely small elements.

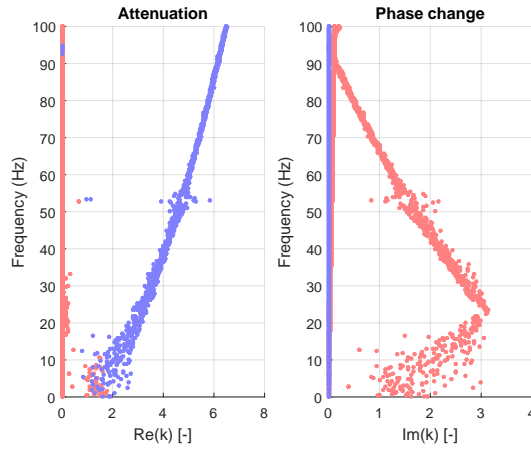


**Figure 3.25:** Dispersion curves from 0 to 100 Hz of the one-dimensional model of an infinite Euler-Bernoulli beam with numerical errors due to the size of the element

When there is not enough number of elements to model the behavior of the unit-cell there can be another type of error as shown in figure 3.26. This figure shows bands gaps which do not exist since it is an undamped system. The explanation for this is that at relative high frequency, the movement of the unit-cell is complex in comparison with the number of degrees of freedom of the model.

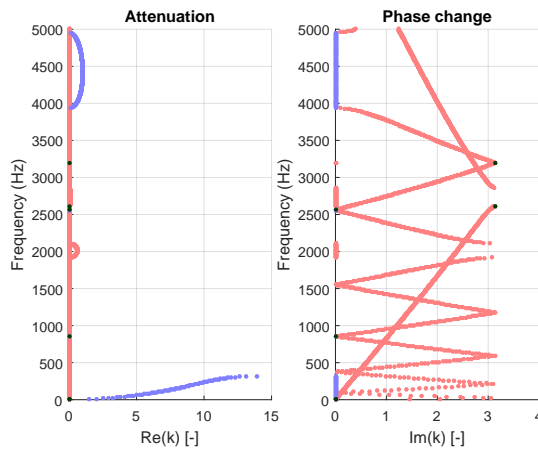


**Figure 3.26:** Dispersion curves from 0 to 5000 Hz of the one-dimensional model of an infinite Euler-Bernoulli beam with discretization errors

Another type of error can be presented due to the element selection. Figure 3.27 shows the dispersion diagram of a three-dimensional model of a beam with SOLID185 elements. The first frequency is observed above 24 Hz which is incorrect according to the results shown previously. Knowing from the beginning of the analysis that the problem will be bending dominated, the enhanced strain formulation should be activated by the user in order to get accurate results.

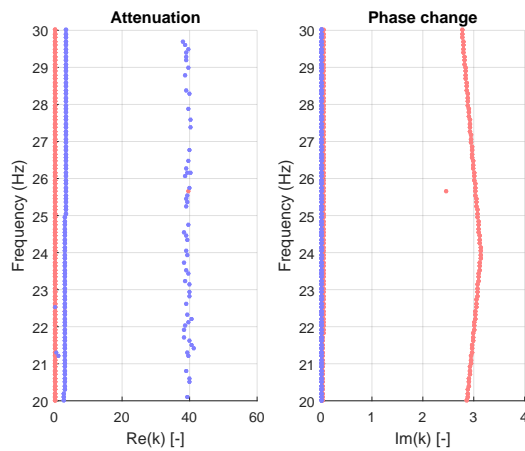


**Figure 3.27:** Dispersion curves from 20 to 30 Hz of the three-dimensional model of an infinite Euler-Bernoulli beam with errors due to the element selection

## 4 Numerical experiments

This section aims to numerically explore the dispersion properties of the so-called acoustic black hole. Numerous numerical simulations are performed to visualize the effect on the manipulation of its main geometrical and physical parameters.

### 4.1 Analysis of an acoustic black hole in one dimension

Mechanical vibration analysis plays a key role in predicting potential vibration problems in engineering designs. When problems are predicted, designs can be modified to mitigate vibration before systems are manufactured. However, many vibration studies are carried out after having the system manufactured so that the vibration problems must be handled using passive methods.

Traditional passive methods to control vibrations rely on the manipulation of the amount of mass, damping and stiffness of the system. An example is the tuned mass damper (TMD), which can be installed into a system to avoid excessive vibration in a variety of engineering problems. Another examples are the so-called metamaterials which are artificial materials made as a combination of two or more materials in a way that form a periodic structure, offering different wave propagation characteristics such as band gaps.

One type of metamaterial that has been developed in the last years, as lightweight method to effectively attenuate bending wave vibrations in beams and plates, is a periodic material with exponential-like circular tapers, called acoustic black hole. Figure 4.1 shows the basic profile of an acoustic black hole and its design parameters [Zhu 2014].

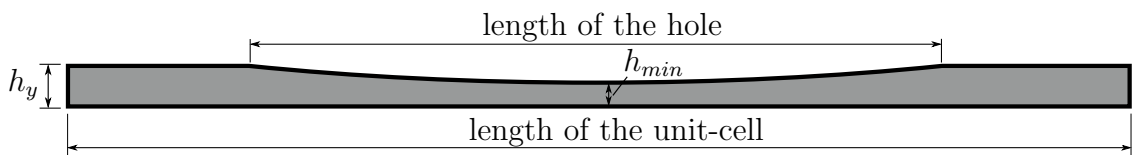


**Figure 4.1:** Main design parameters of an acoustic black hole

The most critical design parameter is the exponential taper coefficient  $exp$ , which is a progression of the profile from a straight wedge-type (low  $exp$ ) to a curvilinear-type profile (high  $exp$ ) as it is shown in figure 4.2.

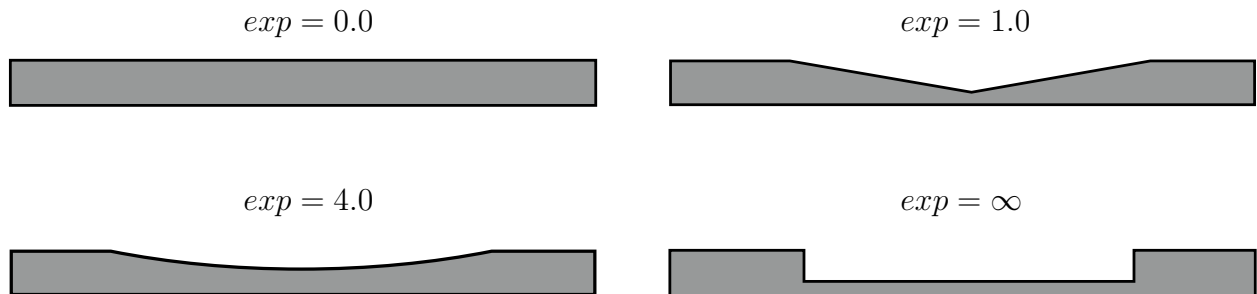


**Figure 4.2:** Acoustic black hole with different values of exponential taper coefficient  $exp$

The main principle of this kind of materials is the gradual decrease of velocity of the incident wave as the thickness of a beam or plate decreases. If the thickness decreases smoothly to zero, the wave velocity decreases and stops without being reflected. The condition for providing zero wave reflection is hardly fulfilled since it is needed a zero residual thickness, which is impossible in reality. Therefore, the additional layer provides the unit-cell with extra stiffness for a very small value of residual thickness and compensates the attenuation that is not given by the unit-cell itself [Krylov 2012]. The complete theory of acoustic black holes can be found in [Krylov 2012].

Figure 4.3 shows an acoustic black hole with a viscoelastic damping layer for further energy dissipation and vibration reduction. In general, acoustic black holes require very small amounts of added damping materials, in comparison with traditional methods which add thick layers of material.

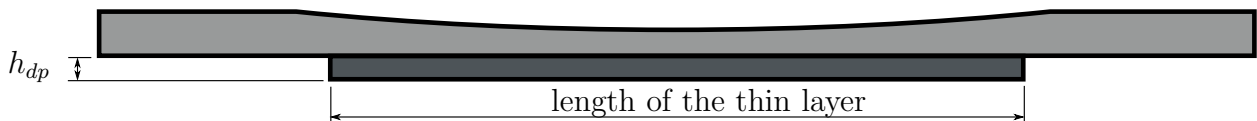


**Figure 4.3:** Acoustic black hole with an additional thin layer

The first experiments are carried out to see the effect of the exponential taper coefficient of an undamped titan unit-cell without the additional thin layer. Table 4.1 summarizes the general characteristics of the undamped unit-cell.

Property	Symbol	Value
Length of the unit-cell	$L_x$	0.3 m
Length of the hole	$dia$	0.2 m
Thickness of the unit-cell	$h_y$	3 mm
Residual thickness	$h_{min}$	1 mm
Young's modulus	$E$	104 GPa
Poisson's ratio	$\nu$	0.31
Density	$\rho$	4429 kg/m <sup>3</sup>

**Table 4.1:** Material properties and dimensions of a one-dimensional titan acoustic black hole

Figure 4.4 shows the dispersion curves of models with different values of exponential taper coefficient. Figure 4.4a shows the dispersion relations of a normal beam which can be considered as a black hole with exponential taper coefficient equals to zero. The dispersion relations show several branches in the imaginary part that are associated with propagating bending waves.

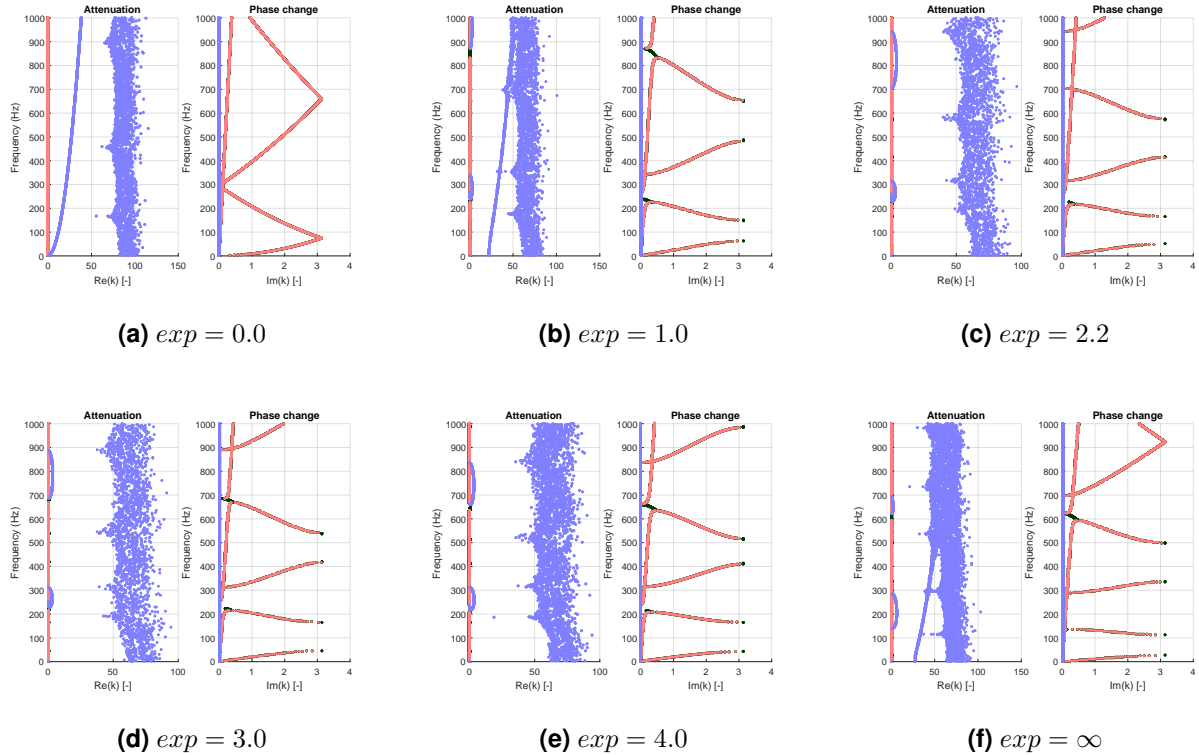


**Figure 4.4:** Dispersion curves from 0 to 1000 Hz of one-dimensional undamped unit-cells with different exponential taper coefficient

As soon as the value of exponential taper coefficient increases, free wave propagation is not possible for certain zones and stop bands can be found. For increasing values of exponential

taper coefficient, the band gaps shift to a lower position. Nevertheless, the amount of shifting is reduced for an increasing value of exponential taper coefficient and limited by the behavior when the exponential taper coefficient equals infinity.

If a layer with material properties described in the table 4.2 is added, the band gaps of the unit-cell tend to be pushed downwards. In order to see this effect, figure 4.5 compares the dispersion curves of the unit-cell with and without additional layer of material.

Property	Symbol	Value
Young's modulus	$E$	0.01 GPa
Poisson's ratio	$\nu$	0.45
Density	$\rho$	1000 kg/m <sup>3</sup>

**Table 4.2:** Material characteristics of the proposed layer

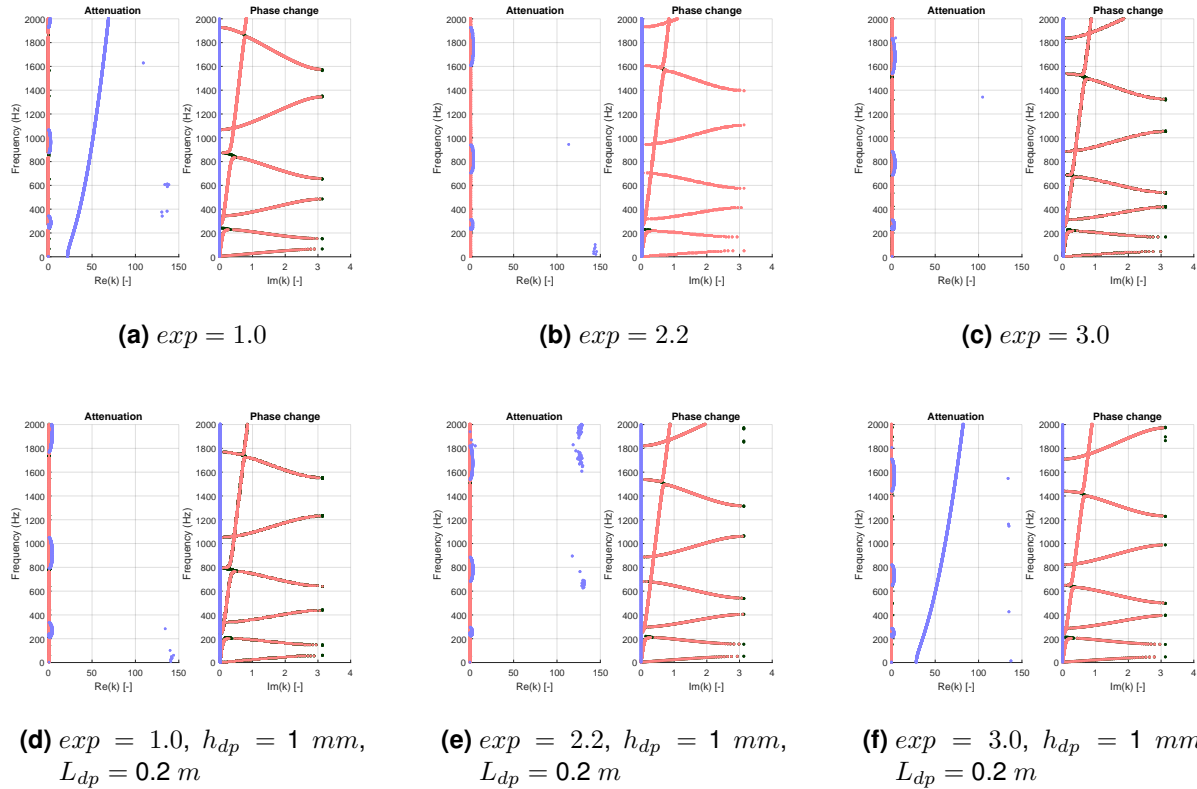


**Figure 4.5:** Dispersion curves from 0 to 2000 Hz of a one-dimensional undamped black hole with and without additional layer of material

In the first row of figure 4.5, it is shown the dispersion diagrams of the unit-cell without additional layer, but with different values of exponential taper coefficient. As it was concluded before, the band gaps shift to a lower position for a higher exponential taper coefficient. In

the second row, the same unit-cell models are used but with an additional layer of material which shifts even further the band gaps.

If the exponential taper coefficient stays in 2.2, the effect of increasing the thickness of the layer  $h_{dp}$  can be analyzed. In figure 4.6 is shown that for increasing thickness, the shifting increases even further. A similar effect can be realized when the length of the layer increases. Therefore, the combination of the normal profile and a layer may result in effective damping systems for flexural vibrations in specific ranges of frequency [Krylov 2012].

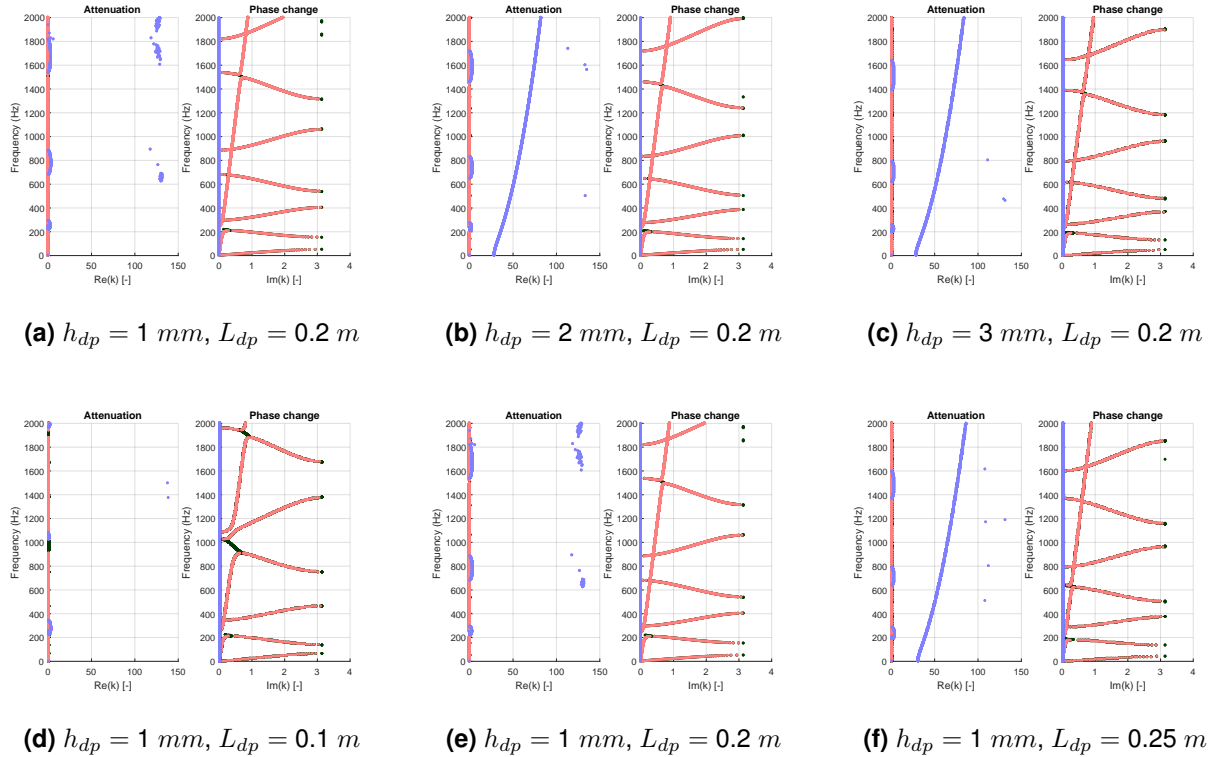


**Figure 4.6:** Dispersion curves from 0 to 2000 Hz of a one-dimensional undamped black hole with exponential taper coefficient equals to 2.2. The figure shows the dispersion curves of unit-cells with different layer properties

As it was mentioned, the propagation of waves depends on the material properties. For example, table 4.3 shows the speed of longitudinal waves in a beam with different materials.

Material	Young's Modulus	Poisson's ratio	Density	$v_l$
Titan	104 GPa	0.31	4429 kg/m <sup>3</sup>	4845 m/s
Steel	210 GPa	0.3	8050 kg/m <sup>3</sup>	5107 m/s
Aluminum	70 GPa	0.33	2700 kg/m <sup>3</sup>	5091 m/s

**Table 4.3:** Material properties of titan, steel, and aluminum

In general, the ratio of the Young's modulus to the density of many materials is similar as shown in table 4.3 when the speed of the longitudinal wave is computed. Therefore, the dispersion curves of the beam with different materials should not change much when they are compared to each other and it should be the same for the acoustic black hole case.

In figure 4.7 is shown the dispersion curves of the unit-cells made of these materials. As expected, the change is almost imperceptible, but it can be seen that the band gaps shift according to the ratio of the Young's modulus to the density.

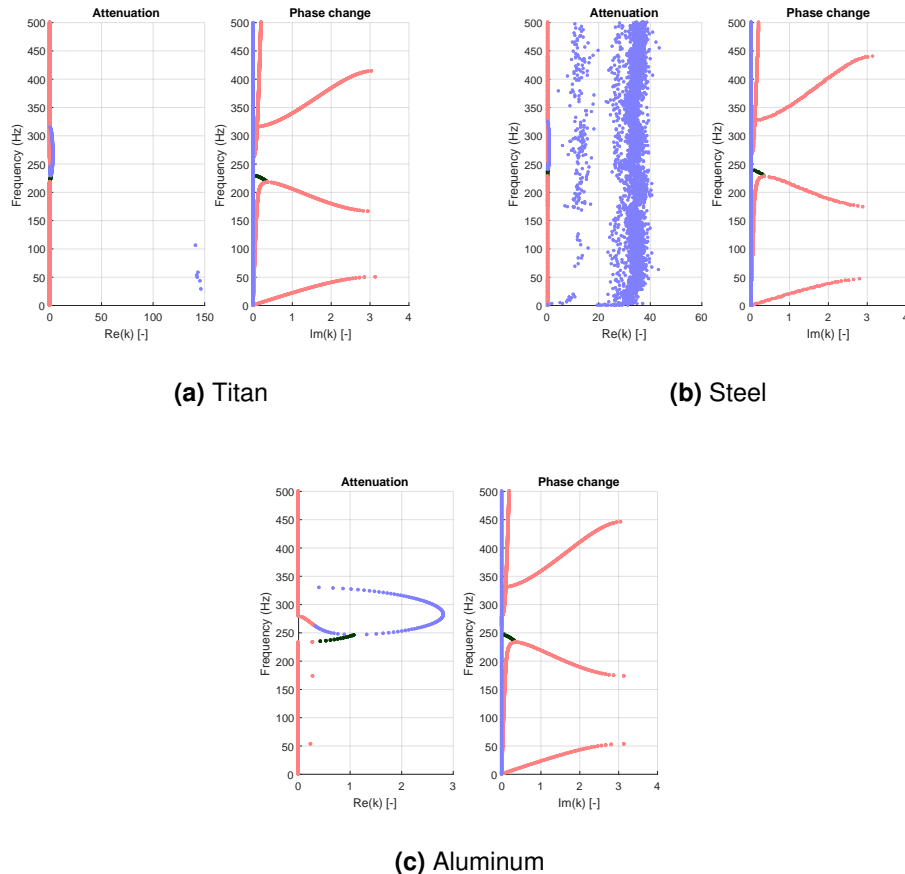


**Figure 4.7:** Dispersion curves from 0 to 500 Hz of a one-dimensional undamped black hole with different materials and exponential taper coefficient equals to 2.2

In order to see the effect of proportional damping as part of the unit-cell, figure 4.8 shows nine dispersion diagrams corresponding to nine unit-cells with different values of damping ratio and exponential taper coefficient. As many practical structural problems that consider proportional damping, alpha damping (or mass damping) is ignored , such that beta damping takes a value over a range for constant damping ratio.

In the first column of the figure, it can be visualized the baseline of the respective undamped unit-cells. In the second and third columns a little bit of damping has been added, which distorts the results. As it was mentioned in the example of a beam with a TMD, the damping tends to distort the results in a way that it becomes difficult to visualize the stop bands. However, if little damping is added, one can see that the attenuation zones get bigger which shows the existence of stronger attenuation along the curves.

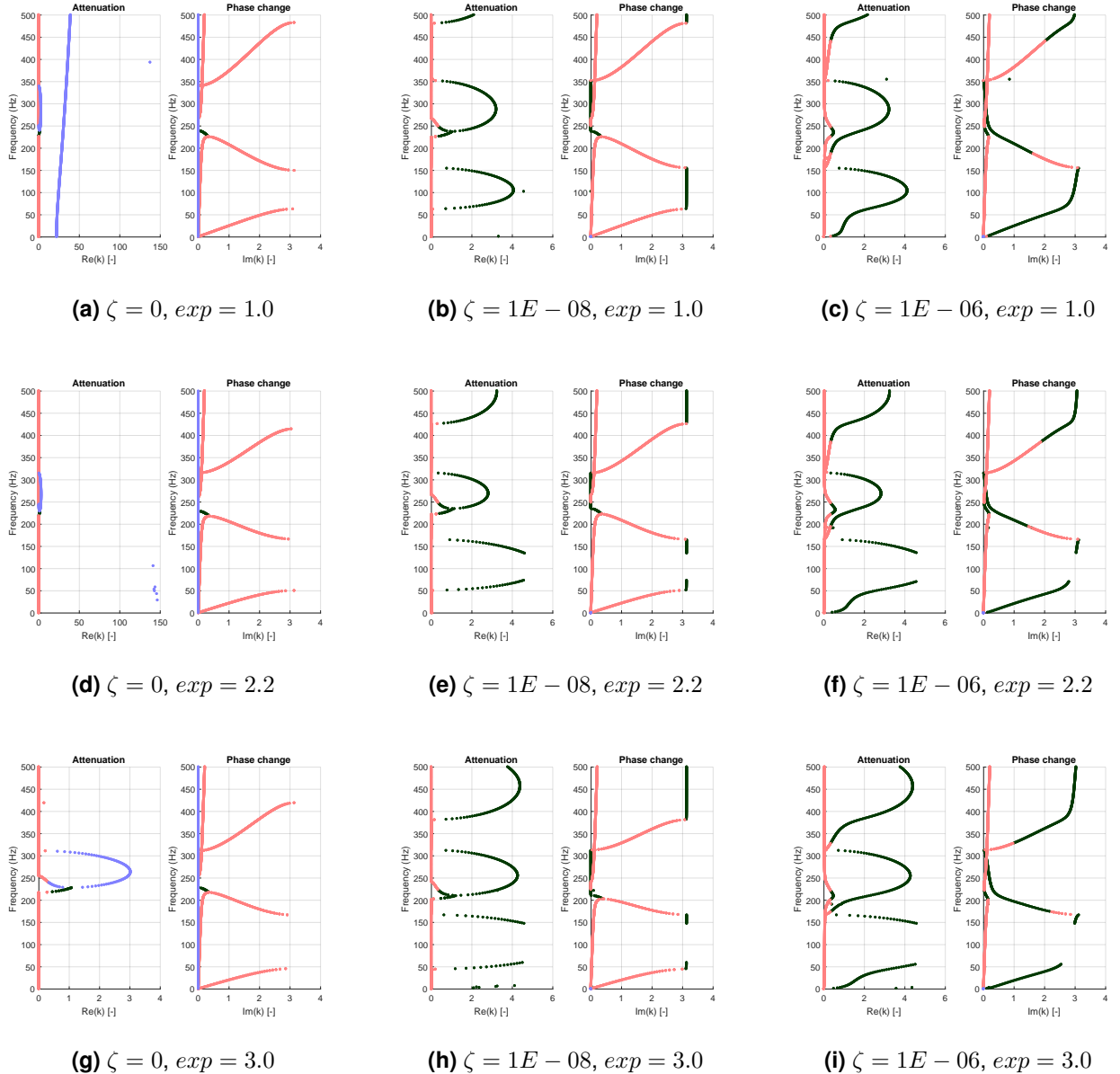


**Figure 4.8:** Dispersion curves from 0 to 500 Hz of a one-dimensional titan black hole with different values of damping ratio and exponential taper coefficient

## 5 Summary and conclusions

This section presents the summary of the thesis, the conclusions and the future work that is necessary to give continuity to this work. The main goals of this thesis were:

- Literature review of unit-cell modeling of periodic structures.
- Creation of a computational tool with ANSYS® and MATLAB® to compute the dispersion diagrams of one-dimensional infinite structures.
- Extension of the tool for two- and three-dimensional periodic structures.
- Evaluation of different designs of acoustic metamaterials to validate the tool.
- Investigation of an acoustic black hole as acoustic metamaterial in one dimension.

During this thesis work, an extensive investigation of the main methods to model infinite periodic structures using the unit-cell approach was presented. Using the unit-cell approach, the behavior of the whole periodic structure can be characterized by one of its elements through its dispersion relations. After the extensive review of the literature, a computational tool to obtain the dispersion relations of one-, two-, and three- dimensional structures was developed in MATLAB®. Once implemented the available numerical methods, the developed work serves as supplementary tool for the design of acoustic metamaterials such as the acoustic black hole.

For a given ANSYS® model of unit-cell, numerical methods based on the wave finite element method are applied. These methods were used to provide a numerical wave description of the dynamic behavior of periodic structures. Different eigenproblems arise, once periodic boundary conditions are applied, which provide the frequency evolution of the wave number so that they can be visualized in diagrams called dispersion curves. The dispersion diagram is produced by sweeping either the frequency or the wave numbers so that after solving the corresponding eigenvalue problem across all the respective parameters involved, the band gaps may be identified in zones of the diagram where no free wave propagation is possible.

From this experience the conclusions and future work are summarized in the following list:

- Due to the fact that ANSYS<sup>®</sup> doesn't provide the dispersion relations for infinite structures, which have to be used to gain insight in the design of acoustic metamaterials, this thesis collects the available methods to model periodic structures using the unit-cell approach. The WFEM-based methods have been developed and used by many authors to investigate infinite periodic structures. Therefore, the second goal was addressed by implementing the wave finite element method in its direct and inverse form as well as the condensed wave finite element method to deal with one-dimensional models. The results that the tool provides were compared with the ones of [Claeys 2013].
- The use of WFEM-based methods is computationally expensive for the analysis of complex structures as the frequency increases. The use of model order reduction techniques such as the condensed wave finite element method, developed by [Zhou 2014], may significantly reduce the time of computation. However, great efforts have to be made not only in developing new numerical techniques but also in optimizing its code implementation.
- MATLAB<sup>®</sup> is used in this thesis due to its simplicity and broad range of tools such as the eig command or the parallel tool box that may speed up the analysis. Although these tools were included in the tool, further implementation have to be made in order to fully take advantage of them.
- The developed tool can analyze models with proportional damping. However, further work has to be made to be capable of including structural damping in the models so that the analysis would be more realistic.
- This thesis focused more in the analysis of one-, two-, and three-dimensional models under one-dimensional wave propagation. Despite the fact that two- and three-dimensional wave propagation methods were implemented, further investigation have to be made to deal with the three-dimensional case.
- Although not analyzed in this thesis, the modes can be determined from these eigen-solutions. However, by computing only the eigenvalues the analysis can be much faster and enough to determine the band gaps.
- The last goal of this thesis consisted in investigating one-dimensional wave propagation in a one-dimensional acoustic black hole. This was addressed by performing numerous experiments on a proposed model and visualizing the changes when the geometric and material properties are modified. With the developed tool one can have a general idea about the wave propagation in this kind of materials. Furthermore, experimental verification must be performed in the future to validate the results.

# A Appendix

## A.1 Graphical User Interface

This section presents the graphical user interface of the tool METAMAT, where all functionalities are grouped visually according to the task they are associated with. The section provides a mock view of the most important aspects of the Graphical User Interface (GUI), along with textual descriptions of their purpose and contents.

In figure A.1, it can be seen the layout of the program METAMAT. The layout is composed of five main parts. The first part is the Model part where the user have the possibility to choose if the analysis is for one-, tow- or three-dimensional wave propagation. In part two is the Analysis part where the user can select between the direct and the inverse approach depending on the analysis to be performed. Part three is only valid when the user selects the direct approach in the Analysis part and it gives the available methods to deal with the model.

In part four the user can introduce the necessary values to start the analysis. There are also three buttons where the first button activates the MATLAB® parpool to speed up the direct analysis, the second button is the restart button which is recommended after having completed one analysis and the "Load input" button which loads the finite element model from ANSYS®. The file can be an input file or a .txt file which contains the APDL code to generate the finite element model.

Finally, part five shows the dispersion or band structure of the analysis, depending whether the user chose between direct and inverse approach. The user may click on the curves to see the values of frequency and wave numbers on a specific point. In case of using the direct approach for undamped models, the color blue represents the evanescence waves, the red color represents the free propagating waves, and the green color the attenuating waves according to the definition of [Mace 2005].

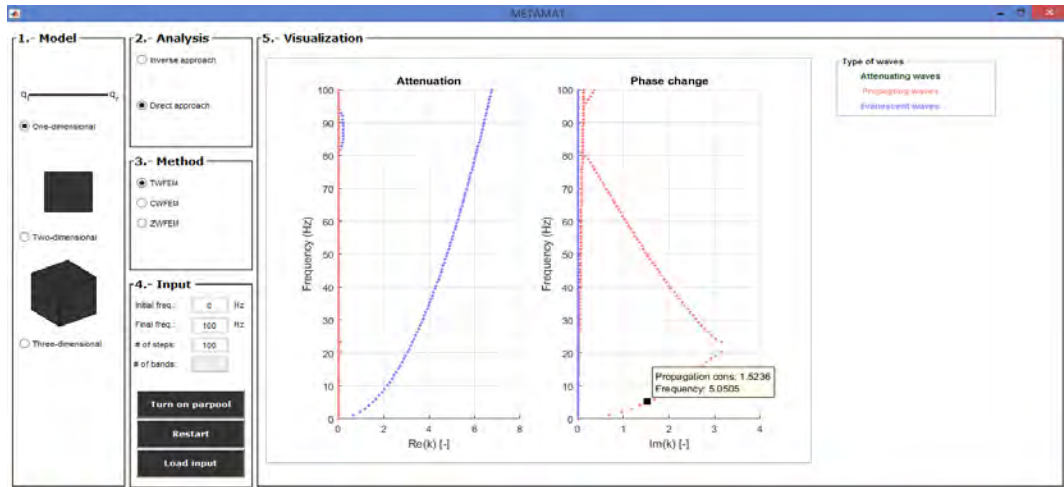


**Figure A.1:** Layout of METAMAT

## A.2 MATLAB<sup>®</sup> code

In this section, all programs developed during this thesis are described and their source code can be found in the enclosed CD. The starting point is the development of an object-oriented strategy which involves the modeling of a program. The standard way to visualize this model is using the Unified Modeling Language (UML). In figures A.2, A.4 and A.3, the simplified UML diagrams of the developed tool are presented.

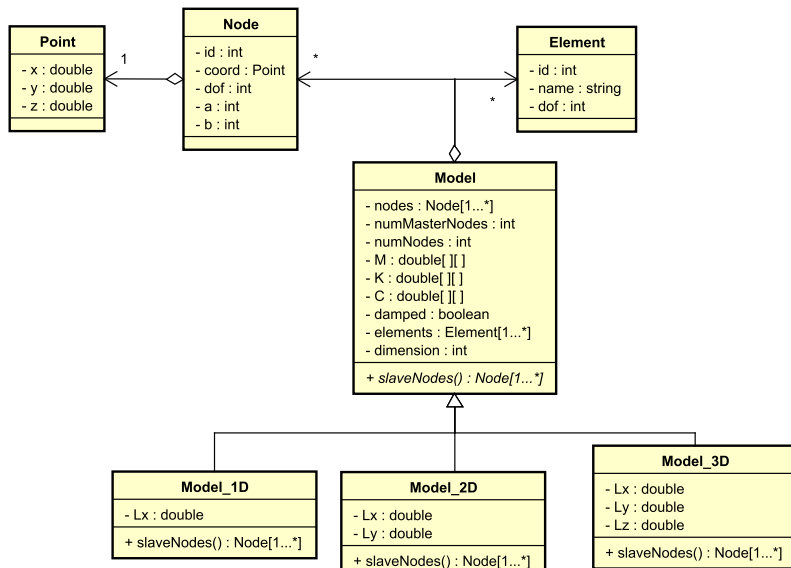


**Figure A.2:** Simplified UML diagram of the implementation of analyzed model

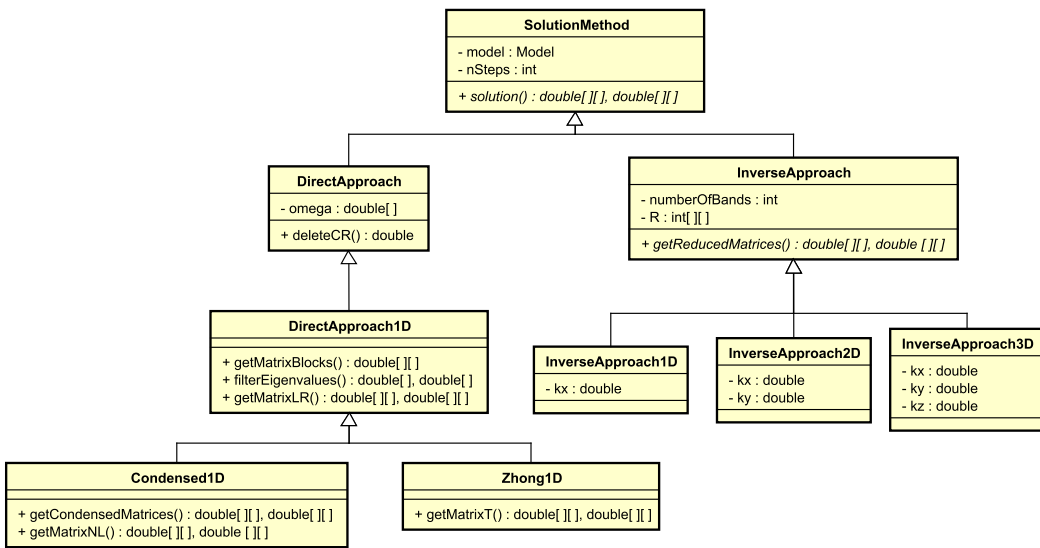


**Figure A.3:** Simplified UML diagram of the implementation of approaches used by the WFEM

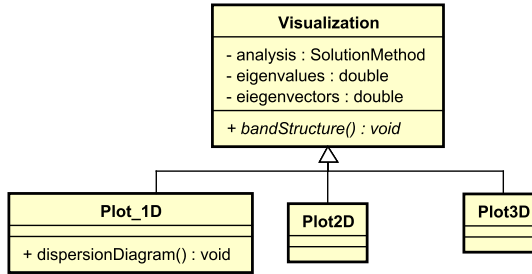


**Figure A.4:** Simplified UML diagram of the implementation of the visualization

**main\_GUI.m:** It is a function which is used to invoke the user interface of the tool. It loads the input file with the Ansys Parametric Design Language (APDL) of the model, obtains the parameters of the desired analysis and provides the visualization of the dispersion diagram or band structure.

### "Code\ReadAnsys" folder

**hb\_to\_msm.m:** It is a program which accepts the name of a file containing a sparse matrix in the Harwell Boeing Sparse Matrix File Format. It reads then that data and returns it as a MATLAB® sparse matrix. This function was retrieved from [Burkardt 2017].

**readRecord\_5.m:** It is a function which obtains the nodal equivalence between the original number of node given in ANSYS® and the distribution of its entries within the matrices generated by ANSYS®. This is performed through the reading of the record 5 of the

file .emat given by ANSYS®. The list is composed of 5 columns of numbers plus a sixth column containing indexes of position [Batailly 2012].

**readCoord.m:** It is a function which obtains the nodes' coordinates from the txt files generated by ANSYS®.

**readRestrictions.m:** It is a function which gets the restrictions on the nodes from ANSYS®.

**readElements.m:** It is a function which obtains the element information from the txt files generated by ANSYS®.

**createElements.m:** It is a function which creates an array of the allowed element objects.

## "Code \Model" folder

**Point.m:** The class Point defines a point with coordinates ( $x,y,z$ ).

**Node.m:** The class Node contains nodal data, such as node number, nodal coordinates, displacements, and the position information of their entries in the mass, stiffness and damping matrices.

**Element.m:** The class Element is a virtual class that allows the definition of each element of the model by name and the involved degrees of freedom.

**Model.m:** It is a class that contains the model information. This information is provided by the input file coming from ANSYS® and includes the matrices, nodal and element information. This class is also the base of more specific objects that describe the model. As a remark, this class have to be modified in line 105 according to the installation path and version of ANSYS®.

**Model\_1D.m:** It is a subclass of the Model class. This class aims to represent model with one directional wave propagation. It accepts models in one- two- and three- dimensions.

**Model\_2D.m:** It is a subclass of the Model class. This class aims to represent model with two directional wave propagation. It accepts models in two- and three- dimensions.

**Model\_3D.m:** It is a subclass of the Model class. This class aims to represent model with three directional wave propagation.

### "Code \Analysis" folder

**WFEM.m:** It is a class that aims to contain the information of the whole analysis. This includes the model, the analysis and the visualization.

**SolutionMethod.m:** It is an abstract class which is the base of other classes that defines the methods of solution given in this thesis.

**DirectMethod.m:** It is an abstract class which is the base of the direct approach.

**DirectMethod1D.m:** It is a class that defines the procedure to apply the traditional one-dimensional WFEM to solve the eigenvalue problem.

**Condensed1D.m:** It is a class that defines the procedure to apply the condensed WFEM to solve the eigenvalue problem.

**Zhong1D.m:** It is a class that defines the procedure to apply the Zhong's method to solve the eigenvalue problem.

**InverseApproach.m:** It is an abstract class which is the base of the inverse approach.

**InverseApproach1D.m:** It is a class that defines the procedure to apply the traditional one-dimensional inverse method.

**InverseApproach2D.m:** It is a class that defines the procedure to apply the traditional two-dimensional inverse method.

**InverseApproach3D.m:** It is a class that defines the procedure to apply the traditional three-dimensional inverse method.

### "Code \Visualization" folder

**Visualization.m:** It is an abstract class that contains the analysis which will be visualized.

**DataPoint.m:** It is a class that contains information about the points that will be plotted, using the direct approach.

**Plot1D.m:** It is a class that provides the methods to plot the band structure for the one-dimensional unit-cell.

**Plot2D.m:** It is a class that provides the methods to plot the band structure for the two-dimensional unit-cell.

**Plot3D.m:** It is a class that provides the methods to plot the band structure for the three-dimensional unit-cell.

## A.3 Python code

In this section, the programs which were provided by the Chair of Structural Mechanics at the Technical University of Munich are described. These programs generate the profiles of the one- and two-dimensional acoustic black hole to be used by ANSYS® as data curves to create a finite element model.

### "Generator" folder

**1DABH\_generator.py:** Generates the coordinates of a one-dimensional acoustic black hole profile in a CSV file format to be used by ANSYS® to create a model according to the user-defined design parameters.

**ABH\_generator.py:** Generates the coordinates of a two-dimensional acoustic black hole profile in a CSV file format to be used by ANSYS® to create a model according to the user-defined design parameters.

## A.4 ANSYS® code

In this section, the benchmark programs which were developed to test the tool METAMAT are described. The programs were created in the Ansys Parametric Design Language to create simple finite element models.

### "Models" folder

**1DBeam.txt:** One-dimensional model of a beam without damping.

**1DBeamWithPunctualMass.txt:** One-dimensional model of a beam with a punctual mass.

**1DBeamWithSpring.txt:** One-dimensional model of a beam with a spring-mass system.

**1DBeamWithTMD.txt:** One-dimensional model of a beam with a TMD.

**2DBeam.txt:** Two-dimensional model of a beam without damping.

**2DUnitCell.txt:** Two-dimensional model of a plate without damping.

**2DUnitcellWithPunctualMass.txt:** Two-dimensional model of a plate with a punctual mass in the middle.

**2DUnitCellWithSpring.txt:** Two-dimensional model of a plate with a spring-mass system in the middle.

**3DBeam.txt:** Three-dimensional model of a beam without damping.

**3DUnitCell.txt:** Three-dimensional model of a unit-cell without damping.

## A.5 Compact disk

The attached CD contains the following contents:

- MATLAB® source code of METAMAT with benchmark models.
- The LATEX files related to this thesis and the relative graphic material.

# Bibliography

- [Batailly 2012] BATAILLY, Alain: Exporting Ansys FEM models into Matlab mass and stiffness matrices / McGill University. 2012. – Research Report. pp. 5-8
- [Bostani 2012] BOSTANI, Ali: *Finite element methods for finding the complex Floquet propagation constant of three dimensional periodic structures*, McGill University, Ph.D. thesis, 2012
- [Brillouin 1953] BRILLOUIN, L.: *Wave propagation in periodic structures*. Dover Publications, 1953
- [Buchschmid 2017] BUCHSCHMID, Martin: *Lecture notes of Structural Dynamics*. Technische Universität München, 2017. – pp. 104-114
- [Burkardt 2017] BURKARDT, John: *Harwell Boeing Sparse Matrix File converted to Matlab Sparse Matrix*. 2017. – URL [http://people.sc.fsu.edu/~jburkardt/m\\_src/hb\\_to msm/hb\\_to msm.html](http://people.sc.fsu.edu/~jburkardt/m_src/hb_to_msm/hb_to msm.html)
- [Claeys 2013] CLAEYS, Claus C.: On the potential of tuned resonators to obtain low-frequency vibrational stop bands in periodic panels. In: *Journal of Sound and Vibration* (2013)
- [Collet 2011] COLLET, Ruzzene: Floquet-Bloch decomposition for the computation of dispersion of two-dimensional periodic, damped mechanical systems. In: *Elsevier* (2011)
- [Farzbod 2010] FARZBOD, Farhad: *Analysis of Bloch formalism in undamped and damped periodic structures*, Georgia Institute of Technology, Ph.D. thesis, 2010
- [Govers 2015] GOVERS, Y.: Validating global structural damping models for dynamic analysis. In: *Technical University of Berlin* (2015)
- [Hussein 2006] HUSSEIN, Mahmoud: Reduced Bloch mode expansion for periodic media band structure calculations. In: *University of Colorado* (2006)
- [Krylov 2012] KRYLOV, V.: Acoustic black holes and their applications for vibration damping and sound absorption. In: *Proceedings of the International Conference on Noise and Vibration Engineering* (2012)
- [Langley 1992] LANGLEY, R. S.: A note on the force boundary conditions for two-dimensional periodic structures with corner freedoms. In: *Journal of Sound and Vibration* (1992)

- [Mace 2005] MACE, Brian: Finite element prediction of wave motion in structural waveguides. In: *Journal of Sound and Vibration* (2005)
- [Manconi 2008] MANCONI, Elisabetta: *Modelling wave propagation in two-dimensional structures using a wave/finite element technique*, University of Parma, Ph.D. thesis, 2008
- [Mead 1995] MEAD, D. J.: Wave propagation in continuous periodic structures. In: *Journal of Sound and Vibration* (1995)
- [Rixen 2017] RIXEN, Daniel: *Lecture notes of Structural Dynamics*. Technical University of Munich, 2017. – pp. 57-61
- [Ruzzene 2010] RUZZENE, Massimo: *FE Based Analysis of Dispersion for 1D and 2D Periodic Structures*. Georgia Institute of Technology, 2010
- [Silva 2015] SILVA, Priscilla: *Dynamic analysis of periodic structures via wave-based numerical approaches and substructuring techniques*, University of Campinas, Ph.D. thesis, 2015
- [Sims 2007] SIMS, N. D.: Vibration absorbers for chatter suppression: A new analytical tuning methodology. In: *Journal of Sound and Vibration* (2007)
- [Sohir 2017] SOHIR, Samsor: *Dynamic analysis of periodic structures*, School of Engineering and Science Aalborg University, Master thesis, 2017
- [Zhong 1995] ZHONG, F. W. W.: On the direct solution of wave propagation for repetitive structures. In: *Journal of Sound and Vibration* (1995)
- [Zhou 2014] ZHOU, Changwei: *Wave and modal approach for multi-scale analysis of periodic structures*, Ecole Centrale de Lyon, Ph.D. thesis, 2014
- [Zhu 2014] ZHU, Hongfei: Phononic Thin Plates with Embedded Acoustic Black Holes. In: *American Physical Society* (2014)